Carbohydrate Polymers 347 (2025) 122587

Contents lists available at ScienceDirect

Carbohydrate Polymers

journal homepage: www.elsevier.com/locate/carbpol

Acidic polysaccharide from the edible insect *Protaetia brevitarsis seulensis* activates antiviral immunity to suppress norovirus infection

Ibukunoluwa Fola Olawuyi [a,e,1], Eun Heo [b,1], Minju Jeong [c], Jae Hwan Kim [b], Jong-Jin Park [d], Jongbeom Chae [e], Subin Gwon [f], Seong Do Lee [e], Hunseong Kim [e], Oyindamola Vivian Ojulari [e], Young-Bo Song [g], Byung-Hoo Lee [g], Bon Bin Gu [e], Soo Rin Kim [a,e], Joon Ha Lee [h], Wonyoung Lee [a,e], Jae Sam Hwang [i], Ju-Ock Nam [a,e], Dongyup Hahn [e,f,*], Sanguine Byun [b,j,**]

[a] *Research Institute of Tailored Food Technology, Kyungpook National University, Daegu 41566, Republic of Korea*
[b] *Department of Biotechnology, Yonsei University, Seoul 03722, Republic of Korea*
[c] *Department of Agricultural Biotechnology, Seoul National University, Seoul 08826, Republic of Korea*
[d] *Food Safety and Distribution Research Group, Korea Food Research Institute, Wanju-gun 55365, Republic of Korea*
[e] *School of Food Science and Biotechnology, College of Agriculture and Life Sciences, Kyungpook National University, Daegu 41566, Republic of Korea*
[f] *Department of Integrative Biotechnology, Kyungpook National University, Daegu 41566, Republic of Korea*
[g] *Department of Food Science & Biotechnology, Gachon University, Seongnam 13120, Republic of Korea*
[h] *Department of Agricultural Biology, National Institute of Agricultural Sciences, Rural Development Administration, Wanju 55362, Republic of Korea*
[i] *MyoTecSci Inc., Seoul 02792, Republic of Korea*
[j] *POSTECH Biotech Center, Pohang University of Science and Technology (POSTECH), Pohang 37673, Republic of Korea*

ARTICLE INFO

Keywords:
Insect larvae
Polysaccharides
Structure
Immunomodulation
Norovirus

ABSTRACT

Edible insects are gaining attention as potential nutraceutical sources with immunomodulatory properties. This study reports purification and structural characterization of polysaccharides from *Protaetia brevitarsis seulensis* larvae (PBSL) with antiviral activity against murine norovirus. Four polysaccharide fractions purified from PBSL water extracts exhibited varying molecular weights (458.5–627.3 kDa) and monosaccharide compositions, including glucose (42.4–99.2 %), galactose (5.9–13.9 %), rhamnose (0.7–18.7 %), arabinose (3.8–5.4 %), and glucuronic acid (0–15.3 %). The immunomodulatory activity, assessed by interferon-β (IFN-β) production, positively correlated with higher galactose, mannose, rhamnose, and uronic acid contents. Among the fractions, PBS-P, eluted with 0.5 M NaCl, demonstrated superior *in vitro* antiviral activity with IFN-β production exceeding 8-fold compared to other fractions and 82-fold higher than PBSL water extract, confirming it as the main antiviral active component. Structural analysis revealed PBS-P backbone consisted of α-(1 → 4)-D-Glc*p*, α-(1 → 4,6)-D-Glc*p*, α-(1 → 4)-D-Glc*p*A, α-(1 → 3)-D-Gal*p* and α-(1 → 4)-D-Man*p* residues, and branched chains of α-D-Glc*p*-(1→, and α-L-Ara*p*-(1 → 2)-α-L-Rha*p*-(1 → residues. PBS-P suppressed norovirus replication by stimulating IFN-β, TNF-α, and activating NF-κB, STAT1/2, and TBK1-IRF3 pathways, and its oral administration reduced viral loads in infected mice intestines. This study provides the first report on the detailed structural feature of polysaccharide from an edible insect and its antiviral mechanism, highlighting its potential as a new antiviral agent.

1. Introduction

Polysaccharides are abundant carbohydrate polymers found in plants, animals, algae, and microorganisms (Tabarsa et al., 2020). They consist of long chains of monosaccharide units linked by glycosidic bonds and, depending on their structural units, exhibit diverse structural characteristics that can influence their biological properties (Huang et al., 2023). Extensive research has demonstrated the potential of polysaccharides as nutraceuticals, such as antioxidative (Maity et al., 2017), anti-cancer (Qi et al., 2020), anti-inflammatory (Huang et al.,

* Correspondence to: D. Hahn, School of Food Science and Biotechnology, College of Agriculture and Life Sciences, Kyungpook National University, Daegu 41566, Republic of Korea.
** Correspondence to: S. Byun, Department of Biotechnology, Yonsei University, College of Life Science and Biotechnology, Seoul 03722, Republic of Korea.
E-mail addresses: dohahn@knu.ac.kr (D. Hahn), sanguine@yonsei.ac.kr (S. Byun).
[1] These authors contributed equally to this work.

https://doi.org/10.1016/j.carbpol.2024.122587
Received 28 February 2024; Received in revised form 15 July 2024; Accepted 6 August 2024
Available online 8 August 2024

2023), antinociceptive (Shi et al., 2023), immunomodulatory (Manna et al., 2017) and antiviral (Akbari et al., 2022) activities of polysaccharides, with minimal toxicity and side effects observed. Moreover, these biological effects of polysaccharides are influenced by their structural characteristics, including molecular weight, monosaccharide composition, glycosidic linkages, side chain branching, and degree of polymerization, which can vary depending on the polysaccharide source.

The exploration of new polysaccharides from unconventional sources, such as edible insects, has gained significant interest (Ohta et al., 2016). *Protaetia brevitarsis seulensis* larva (PBSL), an edible insect consumed in Asian countries, has been recognized as a health-promoting functional food ingredient (Kwon et al., 2013). Previous studies have reported various bioactivities of PBSL extracts, including neuroprotective effects against trimethyltin-induced seizures and hippocampal neurodegeneration (Lee et al., 2017), protective effects against receptor activator of nuclear factor-κB ligand-induced osteoclastogenesis (Choi et al., 2023), shielding effects against carbon tetrachloride-induced hepatotoxicity (Kang et al., 2012), antithrombotic effects against ferric chloride-induced thrombosis (Lee et al., 2017), and immune modulation effects (Lee et al., 2023). However, the main bioactive constituents in PBSL are yet unknown. Previous studies have attributed the immunomodulatory effects of PBSL extract to the presence of alkaloids (Lee et al., 2017) and water-soluble proteins (Lee et al., 2023). However, the potential bioactivities of polysaccharides from PBSL remain unexplored despite their common presence in edible insect extracts (Ali et al., 2018; Ohta et al., 2014). In addition, when exploring new polysaccharides with potential antiviral potency, it is essential to establish comprehensive structural analyses, elucidate specific molecular interactions, and conduct animal studies to confirm their effectiveness before potential clinical translation, which is lacking in previous studies.

Noroviruses are the leading cause of infectious gastroenteritis worldwide, with a significant global burden of infections and deaths annually (Atmar et al., 2018). The primary mode of transmission is through the fecal-oral route, human-to-human contact, or consumption of contaminated food, and is more severe in children, the elderly, and immunocompromised patients (Cho et al., 2016). Despite extensive efforts, there are currently no approved drugs or vaccines against norovirus infections. Also, owing to the limitations of cultivating and experimentally utilizing human norovirus, researchers have turned to the murine norovirus (MNV) as an alternative model for norovirus studies (Karst et al., 2014). The innate immune response to norovirus infection heavily relies on type 1 interferons (IFN-α and IFN-β) (Mboko et al., 2022). The antiviral effects of type 1 IFN are mediated through the downstream transcription factor, signal transducer and activator of transcription 1 (STAT1), ultimately inducing the expression of interferon-stimulated genes (ISGs) that suppress virus replication (Mboko et al., 2022).

Polysaccharides have been reported to exhibit antiviral properties by activating the innate immune response through interactions with specific receptors on immune cells and modulating various signaling pathways, making them promising candidates for developing novel therapeutic interventions against viral infections (Zarubova et al., 2021). These complex carbohydrates have shown efficacy against various viruses, including herpesviruses, hepatitis viruses, influenza viruses, human papillomavirus, cytomegalovirus, and coronaviruses (Claus-Desbonnet et al., 2022). The antiviral mechanisms of polysaccharides involve direct virus inhibition, enhancement of host immune responses, and modulation of cellular signaling pathways (Andrew & Jayaraman, 2021; Mohanta et al., 2023). For instance, acidic polysaccharide from *Houttuynia cordata* was shown to reduce the residual infectivity of murine norovirus-1 (MNV-1) by altering the morphology of the viral particles, thereby inhibiting virus penetration and internalization into host cells (Cheng et al., 2019). However, there are no reports on the antiviral effects of polysaccharides from PBSL against virus infections, especially murine norovirus. Therefore, the present study aimed to characterize the structure of a polysaccharide purified from PBSL extract and investigate its immunomodulatory effects on MNV infection. Furthermore, we examined the cytokine secretion and signaling pathways involved in the antiviral activity of this polysaccharide and conducted an *in vivo* study to validate its potential as a therapeutic strategy against norovirus infections. Our research provides a better understanding of the structure-activity relationship of PBSL-derived polysaccharides and their potential as natural antiviral agent.

2. Materials and methods

2.1. Animal materials and reagents

The dried powder of PBSL used in this study was sourced from Iksan Gumbeng-I farm (Iksan, Korea). PBSL were maintained at the insect rearing facilities of National Institute of Agricultural Sciences (Wanju, Republic of Korea). The larvae were reared on fermented oak sawdust in a constant rearing room at 25 °C ± 1 °C, under 65 % ± 5 % relative humidity and a 16 h light: 8 h dark photoperiod cycle. The last instar larvae (70 days after hatching) were harvested and washed, boiled, hot air-dried (LD918BS, L'Equip Co., Ltd., Seoul, Korea) at 45 °C for 24 h. The hot air-dried larvae were pulverized (RT-04, Mill Powder Tech., Tainan, Taiwan), passed through a 425 μm aperture sieve (Chung Gye Sang Gong Sa, Seoul, Korea) to obtain a fine powder, and stored in an airtight bag (-20 °C). The hot air-dried powder was used for aqueous extraction and polysaccharides purification. Monosaccharide and molecular weight standards (HPLC grade) were purchased from Sigma-Aldrich (St. Louis, MO, USA). DEAE-Sepharose employed for column chromatography and deuterium oxide (D_2O) for NMR analysis were acquired from Sigma-Aldrich. All other chemicals and reagents used were of analytical grade. Antibodies to STAT1 (#14995), p-STAT1 (#8826), STAT2 (#72604), IκBα (#4812), p-IκBα (#2859), NF-κB (#8242), p-NF-κB (#3033), TBK1 (#3013), p-TBK1 (#5483) and p-IRF3 (#4947) were purchased from Cell Signaling Technology (Danvers, MA, USA). Antibodies to p-STAT2 (#07–224) were purchased from Sigma-Aldrich (St. Louis, MO, USA). Antibodies to IRF-3 (#SC-33641) and β-actin (#SC-47778) were obtained from Santa Cruz Biotechnology Inc. (Dallas, TX, USA).

2.2. Extraction and purification of polysaccharide from PBSL

Polysaccharide was extracted from PBSL and purified following a previous study (Liu, Tang, et al., 2021), with slight modifications, as illustrated in **Fig. S1**. In brief, 500 g of dried larvae powder was combined with 2 L of distilled water in a glass flask and placed in a water bath (GO-90 W, Jeio Tech, Daejeon, Korea) at 60 °C for 6 h. After centrifugation (4000 rpm, 20 min), the supernatant obtained was concentrated using a rotary evaporator and an aliquot was lyophilized to obtain the hot water extract (PBSE, 34 % g/g). The remaining part was mixed with three volumes of 95 % ethanol to precipitate crude polysaccharide for further purification (8 % g/g). The precipitated polysaccharide mass was redissolved in distilled water and subjected to Sevag deproteinization ($CHCl_3$/BuOH = 5:1, *v*/v) three times, followed by dialysis (13 kDa MWCO) in water for 48 h. The resulting solution was subsequently lyophilized (FDS8518, Ilsin BioBase Co. Ltd., Dongducheon-si, Korea), yielding deproteinized polysaccharide (3 % g/g).

Subsequently, the polysaccharide was purified and fractionated using ion exchange chromatography on a DEAE-Sepharose fast-flow column (6 cm × 60 cm). The column was eluted with deionized water (DI) and NaCl solutions (0.1 M, 0.3 M, and 0.5 M) at a 2 mL/min flow rate using a peristaltic pump (LEPP 150F, Labscitech Inc., California, USA). Fractions were collected in tubes using an automatic fraction collector (M2110, Bio-Rad Laboratories, Inc., CA, USA). The

polysaccharide content in each collected fraction was monitored by the phenol-sulfuric acid method. Subsequently, the four purified fractions were lyophilized after dialyzing (13 kDa, 48 h) and stored in air-sealed tubes at −20 °C for further analyses.

2.3. Chemical and structural characterization of polysaccharides

2.3.1. Monosaccharide composition analysis

The monosaccharide composition of the polysaccharide samples was analyzed using HPLC, following hydrolysis and derivatization. Polysaccharide samples (5 mg/mL) were hydrolyzed with 2 M trifluoroacetic acid (TFA) in an autoclave at 120 °C for 1 h, and TFA was subsequently removed from the hydrolysates by adding methanol and evaporating under vacuum using a rotary evaporator. The hydrolyzed samples and standard compounds were dissolved in HPLC ultra-pure water and subjected to 1-phenyl-3-methyl-5-pyrazolone (PMP) derivatization following the method described by Dai et al. (2010). Excess PMP was eliminated by extracting with chloroform five times, and the upper aqueous layer was collected, filtered using a syringe membrane (0.45 μm), and then subjected to HPLC analysis for the quantification of constituent sugars. A UV/VIS HPLC system (UV-2075 plus, Jasco International Co., Ltd., Tokyo, Japan), equipped with an Athena C18 reverse-phase column (250 mm × 4.6 mm, 5 μm, CNW Technologies, Dusseldorf, Germany), was utilized for chromatographic separation under gradient elution with solvent A (8 % acetonitrile in 0.1 M ammonium acetate buffer, pH 5.5) and solvent B (30 % acetonitrile in 0.1 M ammonium acetate buffer, pH 5.5), as previously described by Stepan and Staudacher (2011). The detection wavelength was set at 245 nm, the injection volume was 20 μL, the flow rate was 0.8 mL/min, and the column temperature was maintained at 30 °C.

2.3.2. Molecular weight analysis

The weight-average molecular weight (Mw) and number-average molecular weight (Mn) measurements were conducted using an Ultimate 3000 HPLC Agilent 1100 equipped with a refractive index detector Dionex HPLC Ultimate 3000 RI System, (Thermo Fisher Scientific, Waltham, MA, USA). The separation was performed on Ultrahydrogel 120, 500, and 1000 columns (Waters, Milford, MA, USA) maintained at 40 °C. Polysaccharide solutions (10 mg/mL) were prepared in aqueous 0.1 M sodium azide, and a 50 μL volume was injected. Column elution was carried out using 0.1 M sodium azide buffer at a flow rate of 1 mL/min. Calibration curves were established using Pullulan standard set known molecular weights (P-342, P-10000, P-48800, P-113000, P-210000, P-393000, and P-805000 Da), and data analysis was performed using Chromeleon 6.80 Extension-pak software (Sunnyvale, CA, USA).

2.3.3. Carboxyl reduction and methylation analyses

Prior to methylation, carboxyl groups in the PBS-P polysaccharide were reduced to prepare the reduced product (PBS-PR), following the protocol by Liu, Ye, et al. (2021). 20 mg of PBS-P was dissolved in 10 mL distilled water and incubated with 1 mM 1-ethyl-3-(3-dimethyl aminopropyl) carbodiimide (EDC) for 2 h, pH maintained at 4.75 using 0.1 M hydrochloric acid (HCl). After incubation, the reduction was carried out by gradually adding 2 M sodium borohydride ($NaBH_4$) solution using a syringe, and the reaction was allowed to proceed at room temperature for 1 h, pH kept at 7.0 with 4 M HCl. The resultant solution was dialyzed (3.5 kDa, 24 h) against distilled water and lyophilized to obtain the reduced polysaccharide (PBS-PR). The reduction process was repeated thrice, and the completion of reduction was confirmed by the sulfamate/*m*-hydroxydiphenyl assay (Filisetti-Cozzi & Carpita, 1991).

Methylation was conducted to determine glycosidic linkage types according to a previous method (Pettolino et al., 2012), with minor modifications. PBS-P and PBS-PR (2 mg) were dissolved in 500 μL of dimethyl sulfoxide (DMSO) and stirred until complete dissolution. Then, 30 mg of sodium hydroxide (NaOH) powder and 200 μL of methyl iodide (CH_3I) were added, and methylation was carried out until the mixture appeared creamy, indicating the reaction was complete. The residual CH_3I was removed by adding 1 mL distilled water and 500 μL of dichloromethane (DCM), followed by vortexing and centrifuging, and the water layer was discarded. The DCM layer was washed twice with 1 mL of water, and the mixture was dried using nitrogen gas (N_2).

The methylated sample was hydrolyzed using 2 M TFA (1 mL) at 121 °C for 1.5 h and dried with N_2 gas after cooling. The hydrolyzed sample was reduced by adding 50 μL of 2 M ammonium hydroxide (NH_4OH) solution and 50 μL of 1 M sodium borodeuteride ($NaBD_4$) in 2 M NH_4OH, allowing it to react for 2.5 h. The sample was then acetylated with 250 μL of acetic anhydride at 100 °C for 2.5 h to convert it into partially methylated alditol acetates (PMAAs). The resulting product was separated and extracted using a two-phase solvent system DCM and distilled water. The extracted product was dried, redissolved in acetone, and analyzed using a GC–MS system (Agilent 7890B—5977B GC/MSD, CA, USA) equipped with a capillary column (60 m × 250 μm × 0.25 μm). The temperature program for the GC–MS was set as follows: the initial column temperature was 50 °C, which was then raised to 300 °C at a rate of 5 °C per min and maintained at 300 °C for 30 min. The methylation result was presented as mol% of each sugar derivative based on peak areas divided by the molecular weights (Fig. S6) of the PMAAs (Pettolino et al., 2012).

2.3.4. Thermal analysis

The thermal behavior of PBS-P was investigated using thermogravimetric analysis (TGA) on an auto-thermogravimetric analyzer (Q500, TA Instruments, New Castle, DE, USA). Approximately 10 mg of PBS-P sample was weighed and sealed in a stainless-steel pan, which was then heated from 20 °C to 600 °C at a heating rate of 10 °C/min under a nitrogen atmosphere with a flow rate of 50 mL/min.

2.3.5. Infrared and NMR structural analyses

The Fourier transform infrared (FT-IR) spectra of the polysaccharide samples were recorded on a Frontier FT-IR Spectrophotometer (Perkin Elmer, Hopkinton, MA, USA). The samples were pressed into pellets with KBr powder and analyzed at a resolution of 4 cm^{-1} for a frequency range of 4000–400 cm^{-1}.

NMR spectra were acquired using a Bruker AVANCE Neo-700 MHz spectrometer (Bruker Billerica, MA, USA) with a 5 mm probe at 298 K. For each sample, 100 mg of polysaccharides was exchanged with D_2O and lyophilized thrice before being redissolved in 1 mL of deuterium oxide (D_2O). The solution was filtered and transferred into NMR tubes. One-dimensional ^1H NMR spectra (64 scans) and ^{13}C NMR spectra (21 k scans), as well as two-dimensional ^1H—^1H correlation spectroscopy (COSY, 32 scans), ^1H—^{13}C heteronuclear single-quantum coherence spectroscopy (HSQC, 128 scans), and ^1H—^{13}C heteronuclear multiple-bond spectroscopy (HMBC, 256 scans) were recorded at 30 °C. NMR spectra were processed using MestReNova (v.14.1.2, Mestrelab Research, Santiago de Compostela, Spain).

2.4. Cell culture

RAW 264.7 cells were purchased from the American Type Culture Collection (Manassas, VA, USA). The cells were maintained in Dulbecco's modified Eagle's media (DMEM; Welgene, Seoul, Korea) supplemented with 10 % fetal bovine serum (Gibco, Waltham, MA, USA) and 1 % penicillin-streptomycin (Corning, NY, USA).

2.5. Cell viability assay

Cell viability was determined using either the Trypan blue assay or the sulforhodamine B (SRB)-based staining assay. For the Trypan blue assay, the cell suspension solution was mixed with Trypan blue stain (Invitrogen, Carlsbad, CA, USA) in a 1:1 ratio after the end of treatment, and the mixture was measured using a Countess® II FL Automated Cell Counter (Invitrogen, Carlsbad, CA, USA). The sulforhodamine B (SRB)

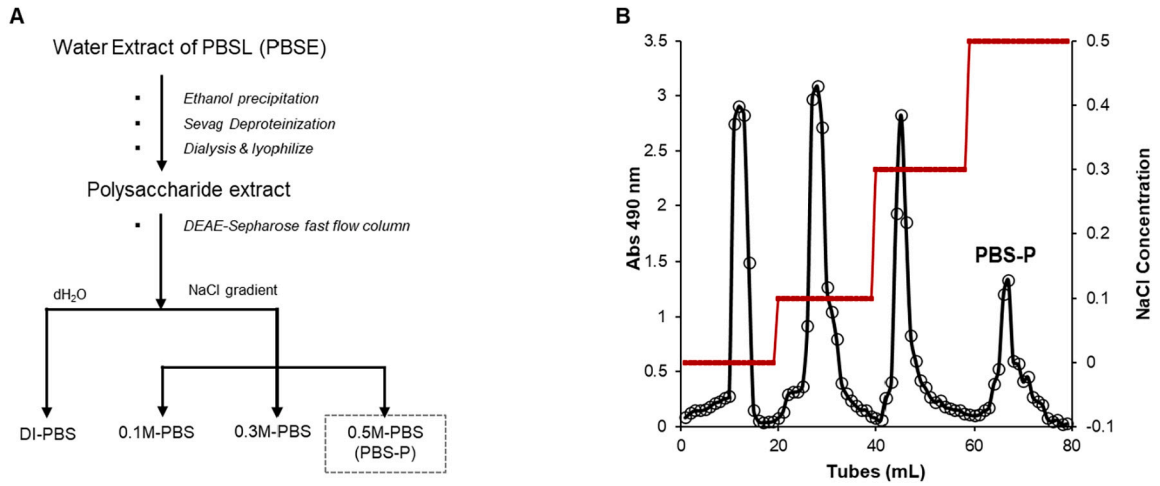

Fig. 1. Purification of immunomodulatory polysaccharides from PBSL. (A) Isolation and purification of polysaccharides from PBSE. (B) Elution profile of fractions separated on DEAE-Sepharose fast flow chromatography.

assay (Sigma-Aldrich) was performed as follows: After the end of treatment, the cells were fixed with 50 % trichloroacetic acid at 4 °C for 1 h, followed by staining with SRB solution for 30 min. Excess dye was then washed off with 1 % acetic acid, and the dye bound to the cells was dissolved in 10 mM Tris. The absorbance of the dissolved dye solution was measured at 554 nm using a Varioskan multimode microplate reader (Thermo Fisher Scientific).

2.6. MNV infection

Infections were carried out at a multiplicity of infection (MOI) of 0.05. RAW 264.7 cells were incubated with the MNV inoculum at 37 °C for 1 h, with gentle shaking every 10 min. Afterward, the MNV inoculum was removed, the cells were washed once with phosphate-buffered saline, and a fresh complete medium with or without PBSL extract or purified polysaccharides was added. The cells were then incubated for 24 h.

2.7. MNV titer assay

MNV titer was quantified by plaque forming assay as previously described (Graziano et al., 2021). RAW 264.7 cells were incubated with harvested media at 37 °C for 1 h. After removing the inoculum, the cells were overlaid with SeaPlaque Agarose (Lonza, Rockland, ME, USA) in complete DMEM for 48 h. Plaques were visualized with crystal violet staining.

2.8. Enzyme-linked immunosorbent assay (ELISA)

The cell culture supernatant was obtained by centrifugation of the medium at 13,000 ×g and stored at −80 °C. The levels of IFN-β and TNF-α were measured using mouse IFN-β and TNF-α DuoSet ELISA kits (R&D Systems Inc., Minneapolis, MN, USA), while the level of IFN-α was measured using a mouse IFN-α ELISA kit (PBL Assay Science, NJ, USA), according to the manufacturer's protocols. The absorbances were measured at 450 nm and 570 nm using the Varioskan multimode microplate reader.

2.9. Real-time quantitative polymerase chain reaction (RT-qPCR)

RNA was isolated using the RNeasy mini kit (Qiagen, Hilden, Germany) according to the manufacturer's protocol. cDNA was synthesized using a ReverTra Ace qPCR RT Master Mix with gDNA Remover (TOYOBO, Osaka, Japan). Real-time PCR was performed with CFX Connect Real-Time System (Bio-Rad, Hercules, CA, USA) and SYBR qPCR Mix (TOYOBO, Japan). To normalize gene expression, Glyceraldehyde-3-phosphate dehydrogenase (GAPDH) was used as a housekeeping gene. The RNA copy number of MNV was quantified as described previously (Wobus et al., 2004). All primers were used as described previously(Gonzalez-Hernandez et al., 2012).

2.10. Western blotting

Proteins from harvested cells were analyzed by western blotting as previously described (Jo et al., 2022). Briefly, after lysed, sample was quantified using BCA assay (Thermo Fisher Scientific). And then equal amount of protein lysates was separated by SDS-polyacrylamide gel electrophoresis and transferred to a nitrocellulose membrane. The membrane was blocked with skim milk and incubated with a specific primary antibody. After incubated with a secondary antibody, protein bands were visualized by WestGlow™ PICO PLUS ECL (Biomax, Seoul, Korea).

2.11. Animal experiments

Animal experiment was approved by the Institutional Animal Care and Use Committee of Yonsei University (IACUC-202305-1676-03) and followed the National Research Council's Guide for the Care and Use of Laboratory Animals. Six-week-old male BALB/c mice were obtained from Orient Bio Inc. (Seongnam, Korea). Mice were accommodated for one week before the experiment in an air-conditioned room at 23 ± 2 °C with 12-h light-dark cycle. The animals were provided with water and mouse chow ad libitum regularly. Mice were divided into 3 groups: (1) control group, (2) MNV-infected group and (3) purified polysaccharide-treated (75 mg/kg of body weight) and MNV-infected group. The purified polysaccharide was orally administered to mice once a day for 8 days. Mice were infected by peroral inoculation with MNV (1×10^8 PFU/100 μL saline). 5 days after inoculation, mice were anesthetized with CO_2 and sacrificed for determination of viral loads in the intestine/colon.

2.12. Statistical analysis

Statistical analyses were performed using GraphPad Prism software (GraphPad Software, La Jolla, CA, USA). For significance analysis, the student's *t*-test was utilized for normally distributed data, while the Mann-Whitney test was performed for non-normally distributed data. Statistical significances were considered at * $p < 0.05$, ** $p < 0.01$ and

Table 1
IFN-β production level by DI-PBS, 0.1 M PBS, 0.3 M PBS, or 0.5 M PBS treatment.

Polysaccharide type	IFN-β concentration (pg/mL)	fold of DI-PBS
Vehicle	0.0	–
DI-PBS	610.4 ± 33.3^{d}	1.00
0.1 M-PBS	2825.0 ± 118.7^{c}	4.63
0.3 M-PBS	4357.7 ± 158.0^{b}	7.14
0.5 M-PBS (PBS-P)	5123.7 ± 244.2^{a}	8.39

The RAW 264.7 cells were treated with purified polysaccharide fractions (20 μg/mL) for 6 h, and the protein levels of IFN-β were measured by ELISA. Values are presented as mean ± SD ($n = 3$), and $p < 0.05$.

Table 2
Monosaccharide composition, molecular weight, and relationship with antiviral properties.

	DI-PBS	0.1 M-PBS	0.3 M-PBS	0.5 M-PBS	Pearson's correlation with IFN-β (r^2)
Monosaccharide composition (mol%)					
Man	0.8 ± 0.0^{d}	1.6 ± 0.0^{c}	3.1 ± 0.1^{b}	5.9 ± 0.1^{a}	0.866
Rha	–	0.7 ± 0.0^{c}	3.0 ± 0.1^{b}	18.7 ± 0.1^{a}	0.730
GlcA	–	–	5.0 ± 0.1^{b}	15.3 ± 0.2^{a}	0.804
Glc	99.2 ± 0.0^{a}	86.4 ± 0.5^{b}	74.0 ± 0.3^{c}	42.4 ± 0.1^{d}	−0.901
Gal	–	5.9 ± 0.6^{c}	11.1 ± 0.1^{b}	13.9 ± 0.0^{a}	0.997
Ara	–	5.4 ± 0.0^{a}	3.8 ± 0.2^{b}	3.8 ± 0.1^{b}	0.679
Molecular characteristics					
Mw (kDa)	627.3 ± 6.2^{a}	458.5 ± 3.3^{c}	577.7 ± 28.5^{b}	478.9 ± 26.8^{c}	−0.561
Mw/Mn	1.7	1.3	1.6	1.4	−0.493

Values are presented as mean ± SD (n = 3), and $p < 0.05$.

***$p < 0.001$.

3. Results and discussion

3.1. Isolation, purification and antiviral activity of PBSL polysaccharides

Hot water extract of PBSL (PBSE) was assessed for its potential antiviral activity. PBSE treatment elevated the level of IFN-β in both mock-infected and MNV-infected groups (**Fig. S2A**). We also observed that PBSE treatment reduced the viral load by 3.5-fold at 20 μg/mL and 6-fold at 100 μg/mL (**Fig. S2B**). These results suggest that PBSE can promote antiviral immunity and enhance host cell resistance against MNV. Since polysaccharides have been recognized as the major active ingredients contributing to the immunomodulatory activity observed in certain functional food sources (Kim, Jeong, et al., 2022; D. H. Kim, Kim, et al., 2022), we isolated and purified polysaccharides from PBSE to evaluate their specific antiviral activity.

Water-soluble polysaccharides were isolated from PBSE and purified through a multi-step process involving ethanol precipitation, deproteinization, dialysis, and lyophilization (Fig. 1A). The purification was then carried out using a DEAE-Sepharose fast-flow column with stepwise elution using deionized water (dH_2O) and NaCl gradient solutions of 0.1 M, 0.3 M, and 0.5 M., Four purified fractions were obtained from crude polysaccharide (1 g): DI-PBS (221 mg), 0.1 M-PBS (278 mg), 0.3 M-PBS (250 mg), and 0.5 M-PBS (239 mg) (Fig. 1B). The purified fractions were evaluated for their ability to induce interferon-beta (IFN-β) production, an important antiviral immune response. ELISA results showed significant differences ($p < 0.05$) in IFN-β induction (610.4–5123.7 pg/mL), with the 0.5 M-PBS fraction exhibiting the highest level, up to 8-fold higher than the least effective fraction (Table 1).

Monosaccharide analysis revealed that all fractions were heteroglycans predominantly composed of glucose (Glc, 42.4–99.2 %), along with varying amounts of mannose (Man), rhamnose (Rha), galactose (Gal), arabinose (Ara), and glucuronic acid (GlcA) (Table 2). DI-PBS and 0.1 M-PBS were neutral polysaccharides, while 0.3 M-PBS and 0.5 M-PBS were acidic polysaccharides containing GlcA (Mehmood et al., 2019). Furthermore, the fractions varied in their molecular weights (458.5 to 627.3 kDa) and molecular distributions (Mw/Mn ratio of 1.3 to 1.7). To further understand the structure-function relationship, the data were subjected to correlation analysis.

Pearson correlation analysis showed a strong negative correlation between IFN-β production and Glc content ($r^2 = -0.901$), and positive correlations with Gal ($r^2 = 0.997$), Man ($r^2 = 0.866$), and GlcA ($r^2 = 0.804$), suggesting that the proportions of these monosaccharide residues directly influence the ability to induce IFN-β. Additionally, molecular weight exhibited a moderate negative correlation ($r^2 = -0.561$) with IFN-β production, indicating that lower molecular weight polysaccharides may be more effective in inducing IFN-β. This finding aligns with previous studies where higher Gal content in acidic heteropolysaccharides exhibited increased immunostimulatory properties in RAW264.7 murine macrophage cells (Tabarsa et al., 2020), and enhanced antiviral activity against MNV-1 (Cheng et al., 2019). Furthermore, the presence of uronic acid in polysaccharides has been positively correlated with enhanced regulation of cytokine secretion and immune-enhancing functions (Wu et al., 2022; Zeb et al., 2021). Based on these results, the higher IFN-β production observed in the 0.5 M-PBS fraction, henceforth referred to as PBS-P, can be attributed to its increased composition of Gal, Man, and GlcA in its heteroglycan structure. Consequently, PBS-P was selected for further structural characterization and antiviral mechanism studies.

3.2. Structural characterization of PBS-P

3.2.1. Monosaccharide and molecular analyses of PBS-P

In detail, PBS-P, categorized by its composition as an acidic heteroglycan, contains Glc, Rha, Gal, GlcA, Man, and Ara with mean values of 41.9 %, 19.7 %, 16.2 %, 15.1 %, 5.9 %, and 4.4 %, respectively (Table 2, **Fig. S3**). The relatively high Rha content is noteworthy, as animals cannot synthesize this sugar de novo (Giraud & Naismith, 2000). Previous studies have discovered the presence of rhamnose in insect pupae extracts, and insects may be able to biosynthesize complex polysaccharides through a unique UDP-synthesis pathway, potentially utilizing external food resources, although this remains unclear (Ohta et al., 2014; Ohta et al., 2016). Our findings confirm the presence of rhamnose in PBS-P, but further investigation would include the elucidation of the exact origin of rhamnose, the specific biosynthetic pathways involved, and the potential role of gut microbiota in polysaccharide synthesis in insects. In addition, investigation on the biosynthesis of polysaccharides in PBSL depending on its feed sources will provide valuable insights into the mechanisms underlying the production of these complex polysaccharides in insects.

Molecular weight analysis was conducted using high-performance size-exclusion chromatography, referencing Pullulan standards. The elution profile of PBS-P (Fig. 2A) exhibited a homogeneous molecular distribution, with a polydispersity index of 1.4 and a calculated mean weight-average molecular weight (Mw) value of 478.9 kDa. Notably, PBS-P appeared as a single symmetrical peak, confirming the purity and homogeneity of the polysaccharide.

3.2.2. Thermal properties of PBS-P

The thermal stability and degradation behavior of PBS-P were investigated using TGA (Fig. 2B). The TGA thermogram revealed four distinct stages of weight loss between 20 °C and 600 °C. The initial weight loss of 5.76 % up to 100 °C was attributed to the evaporation of bound water molecules, which is typical for polysaccharides (Olawuyi &

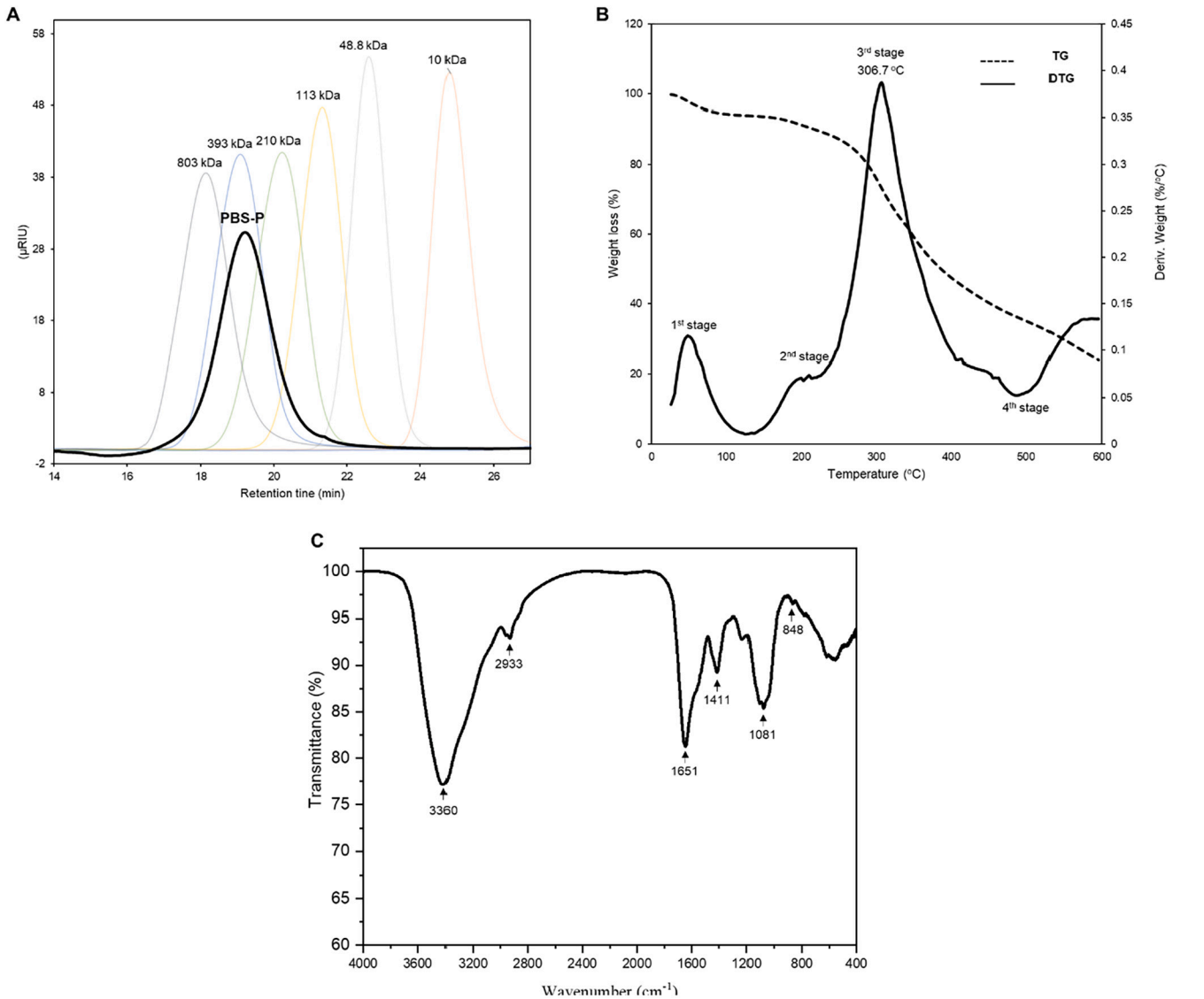

Fig. 2. (A) Molecular weight profile of PBS-P (black line) and pullulan standards (B) Thermogravimetric analysis TGA curve, and (C) FT-IR spectrum of PBS-P.

Lee, 2021). The second stage, around 205 °C, showed a minor weight loss of about 3.76 %, likely due to the degradation of loosely bound side chains of the polysaccharide segments. The major degradation stage, accounting for approximately 55.46 % weight loss, occurred between 210 °C and 360 °C, with a peak degradation temperature of 306.7 °C. This stage involves the cleavage of glycosidic linkages and decomposition of the polysaccharide main chain backbone (Lin et al., 2023), which includes various monosaccharide residues such as glucose, galactose, mannose, and glucuronic acid. This temperature range is consistent with literature reports of thermal depolymerization and glycosidic bond cleavage in polysaccharides above 220 °C (Olawuyi & Lee, 2021). The final weight loss of 10.90 % above 400 °C was attributed to the charring and combustion of residual carbonaceous material. This multi-stage degradation profile highlights the heterogeneous nature of PBS-P and demonstrates its good thermal stability below 200 °C, indicating its suitability for various applications.

3.2.3. *FT-IR analysis of PBS-P*

The FT-IR structural analysis was conducted to complement the monosaccharide results and identify specific structural configurations in

Table 3
Methylation analysis results for PBS-P.

Code	Methylated sugar	Linkage types	Mass fragments (*m/z*)	Molar ratio (%)
A	2,3-Me_2-Glu*p*	→4,6)-α-Glc*p*-(1→	43,59,85,102,118,127,142,162,201,261	15.7
B	2,3,6-Me_3-Glu*p*	→4)-α-Glc*p*-(1→	43,87,99,118,129,142,162,233	49.4
C	2,4,6-Me_3-Gal*p*	→3)-α-Gal*p*-(1→	43,59,74,87,101,118,129,143,161,174,234	9.4
D	2,3,6-Me_3-Man*p*	→4)-α-Man*p*-(1→	43,71,87,102, 118,129,142,162,233	7.6
E	3,4,-Me_2-Rha*p*	→ 2)-α-Rha*p*-(1→	43,72,89,115,131,190	7.3
F	2,3,4-Me_3-Ara*p*	T-α-Ara*p*-(1→	43,59,73,88,101,118,129,162	3.0
G	2,3,4,6- Me_4-Glu*p*	T-α-Glc*p*-(1→	43,71,87,102,118,129,145,162,205	10.1
H	2,3,6-Me_3-Glu*p*	→4)-α-Glc*p*A-(1→	43,87,99,118,129,142,162,233	13.3[1]

[1] %mol derived from 1,4-linked-Glc*p* in PBS-PR.

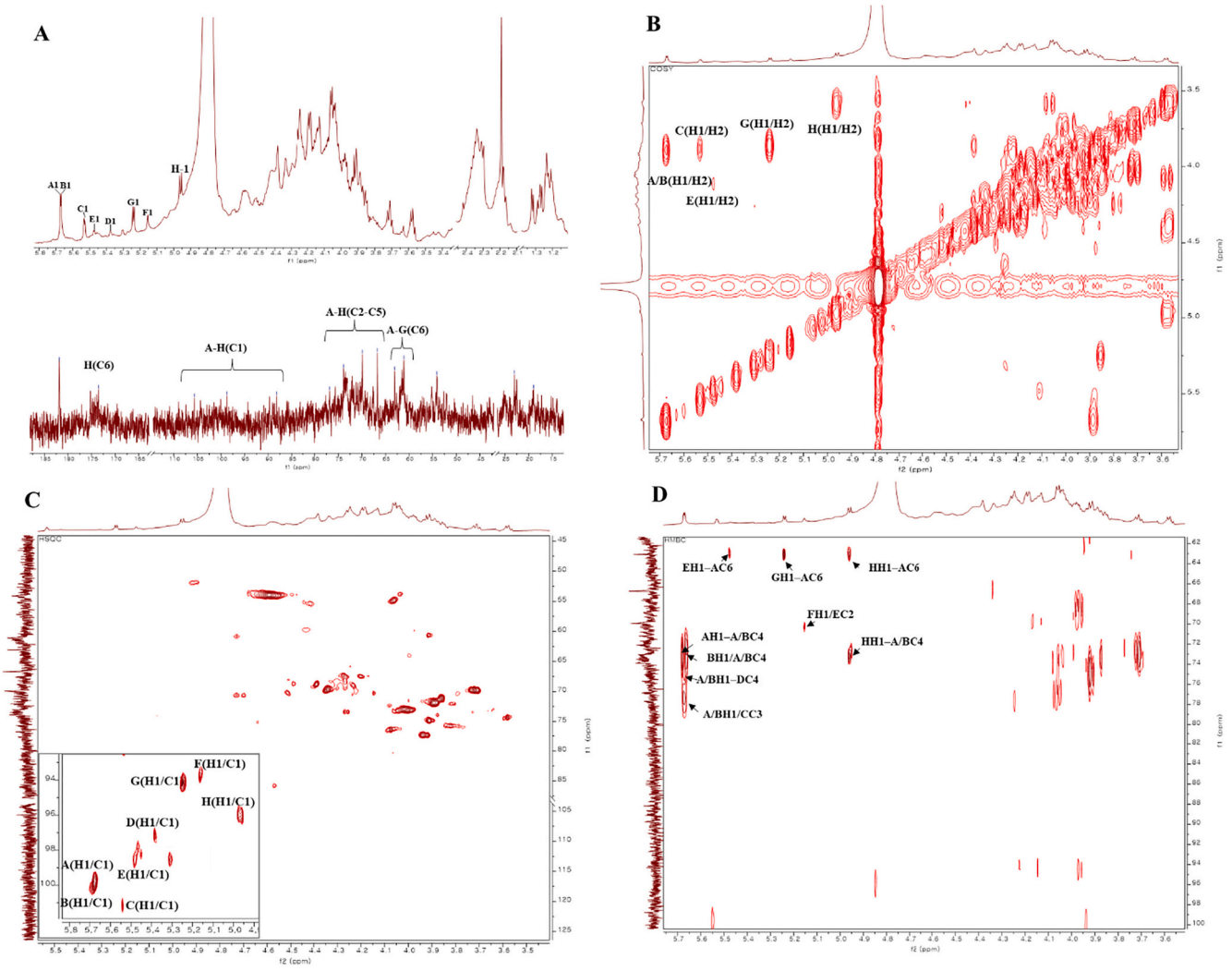

Fig. 3. One-dimensional ^{1}H, ^{13}C (A), Two-dimensional COSY (B), HSQC (C), and HMBC (D) spectra of PBS-P.

PBS-P (Fig. 2C). The broad absorption peaks at 3360 cm^{-1} and the weak peak at 2933 cm^{-1} in the FT-IR spectra can be attributed to the stretching vibration of O—H and C—H bonds, respectively (Yin et al., 2022). Additionally, the absorption peaks at 1651 cm^{-1} and 1411 cm^{-1} are assigned to the asymmetrical and symmetrical stretching vibration of COO−, respectively, confirming the presence of uronic acid (He et al., 2016). Absorption peaks at 1024 cm^{-1}, 1081 cm^{-1}, and 1151 cm^{-1} within the "fingerprint region" of polysaccharides are associated with the stretching vibration of pyranose sugars (Shi et al., 2023). The presence of a single peak at 844 cm^{-1} indicates the exclusive existence of α-linkages in PBS-P (Fig. 2C), unlike other purified fractions (DI-PBS), which contain both α-glycosidic (at 844 cm^{-1}) and β-glycosidic (at 932 cm^{-1}) linkages (**Fig. S4**). Therefore, all sugar residues present in PBS-P are likely to be α-glycosidic configured (Yin et al., 2022).

3.2.4. Glycosidic linkage analysis of PBS-P

To elucidate the glycosidic linkages and identify the presence of uronic acids, methylation analysis was performed on the PBS-P and its carboxyl-reduced form PBS-PR. The profile of PMAAs obtained from GC–MS methylation analysis (**Fig. S5** and **Fig. S6**) are presented in Table 3. The result revealed that PBS-P predominantly exhibited α-linkage types, corroborating the findings from the FT-IR spectrum (Fig. 2C). Seven distinct glycosidic linkage types were identified in PBS-P, with (1 → 4)-α-D-Glc*p* and (1 → 4,6)-α-D-Glc*p* residues being the most abundant, confirming these linkages as main structural components. PBS-PR showed the same glycosidic linkage types as PBS-P, indicating that no new glycosidic linkage was formed during the reduction process. However, a notable increase in %mol of (1 → 4)-α-D-Glc*p* was observed in PBS-PR, suggesting that Glc*p*A is present as (1 → 4)-α-D-Glc*p*A in PBS-P. This confirms that PBS-P is an acidic heteroglycan with a predominant (1 → 4)-linked α-D-Glc*p* backbone, and the presence of (1 → 4,6)-linked α-D-Glc*p* residues indicates branching within the polysaccharide structure. The variations observed in the monosaccharide composition and glycosidic linkage proportions could have resulted from factors inherent to the differences in analytical methods, potential degradation, and incomplete methylation of some sugar linkages present in minor amounts (Liu, Ye, et al., 2021; Sims et al., 2018). To further elucidate the structural orientation of other non-branched and branched residues, as well as terminal units, 2D NMR analyses were conducted.

3.2.5. NMR structural characterization of PBS-P

The anomeric protons (δH) and carbons (δC) were observed through 1D NMR spectra (Fig. 3A). The cluster and overlapping pattern of anomeric δ_H and δ_C signals of sugar residues between 4.96 and 5.68 ppm and 94.06–101.15 ppm, respectively, suggested that PBS-P has a complex and heterogenous structure, typical to heteropolysaccharides (Olawuyi & Lee, 2021; Zeb et al., 2021). Moreover, these signals resonated at δ_H and δ_C regions designated as α-glycosidic regions (Chen et al., 2022), indicating that all residues are α-configurated, in confirmation with the methylation data (Table 3), and FT-IR analysis (Fig. 2B).

Table 4
Summarized HSQC Chemical shifts for PBS-P.

Sugar residues		H1 C1	H2 C2	H3 C3	H4 C4	H5 C5	H6 C6	HMBC
A	4,6)-α-Glc*p*-(1 → 4	5.68	3.88	3.91	4.00	3.73	3.98, 3.85	A/B-4
		99.86	73.88	74.94	73.00	73.43	62.91	
B	4)-α-Glc*p*-(1 → 4	5.66	3.89	3.89	4.02	3.72	3.95,4.15	A/B-4
		99.86	71.93	74.94	73.00	69.78	62.91	
C	3)-α-Gal*p*-(1 → 4	5.54	3.88	3.92	4.27	3.79	3.92, 4.07	A/B-4
		101.15	73.86	77.30	67.42	70.43	60.76	
D	4)-α-Man*p*-(1 → 4	5.39	3.82	4.39	3.93	4.00	4.16	A/B-4
		97.07	75.80	68.92	76.85	63.98	60.97	
E	2)-α-Rha*p*-(1 → 6	5.48	4.15	4.07	4.38	4.20	1.22	A-6
		98.77	70.21	76.44	68.71	67.42	18.21	
F	T-α-Ara*p*-(1 → 2	5.16	4.64	4.70	4.27	4.49		E-2
		93.85	75.15	70.64	73.43	68.71		
G	T-α-Glc*p*-(1 → 6	5.25	3.86	4.08	4.25	3.82	4.05, 4.19	A-6
		94.06	71.07	72.36	65.91	71.93	61.19	
H	4)-α-Glc*p*A-(1 → 4	4.96	3.58	4.34	4.57	4.51		A/B-4
		95.99	74.29	69.57	85.90	70.43	173.55	

Furthermore, the methyl signals near δ_H 1.2 and 2.1 ppm and the δ_C signal around δ 18 and 22 ppm confirmed the presence of the Rha*p* residue and acetylated Glc*p*A residue, respectively (Zhang et al., 2018). Additionally, the δ_C signal at δ173.55 and 181.85 ppm corroborated the presence of the uronic acid in PBS-P.

Based on the correlations observed in 2D NMR COSY (Fig. 3B), and chemical shifts retrieved from HSQC (Fig. 3C) spectra, corresponding $\delta H/\delta_C$ chemical shifts of sugar residues were assigned in Table 4. The cross-peak signals at δ 5.68/99.86 (A), 5.66/99.86 (B), 5.54/101.15 (C), 5.39/97.07 (D), 5.48/98.77 (E), 5.16/93.85 (F), 5.25/94.06 (G), and 4.96/95.99 (H) ppm were attributed to δH-1/δC-1 of sugar residues, namely →4,6)-α-Glc*p*-(1→, →4)-α-Glc*p*-(1→, →3)-α-Gal*p*-(1→, →4)-α-Man*p*-(1→, →2)-α-Rha*p*-(1→, T-α-Ara*p*-(1→, T-α-Glc*p*-(1→, and α-Glc*p*A-(1→, respectively. The H/C signal at 4.59/53.88 ppm, corresponding to *O*-acetyl proton peaks at 2.19 ppm as identified by COSY, is attributed to acetylated Glc*p*A residues (Olawuyi & Lee, 2021). Other $\delta H/\delta_C$ signals of residues were assigned based on HSQC spectra in combination with COSY correlations and literature data (Table 4).

The HMBC correlation spectra further revealed the sequence of linkages in the backbone structure of PBS-P (Fig. 3D). Cross-peaks from H1 of residues A (δ_H 5.68 ppm) and B (δ_H 5.66 ppm) to their respective C4 residues A/B (δ_C 73.0 ppm) revealed the predominant sequence of

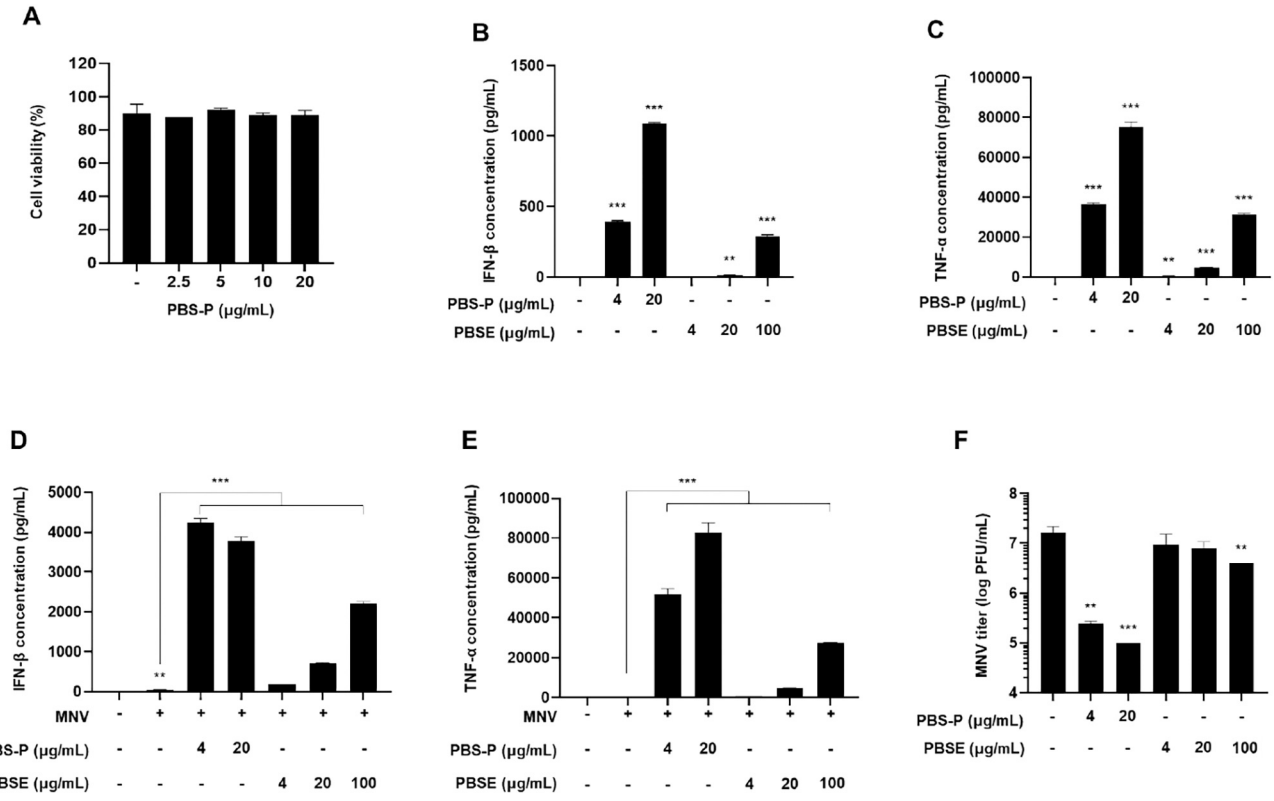

Fig. 4. Antiviral activity of PBS-P against MNV compared with PBSE.
The RAW 264.7 cells were treated with PBS-P or PBSE, respectively, for 24 h. (A) Cell viability of PBS-P treatment was measured by Trypan blue assay. Protein levels of (B) IFN-β and (C) TNF-α were measured by ELISA. (*E*-G) The cells were infected with MNV (MOI of 0.05) and treated PBS-P or PBSE, for 24 h postinfection. And the protein levels of (D) IFN-β and (E) TNF-α were measured by ELISA. (F) MNV titers were determined using a plaque forming assay. Data are shown as mean ± SD. $^{**}P < 0.01$ and $^{***}P < 0.001$.

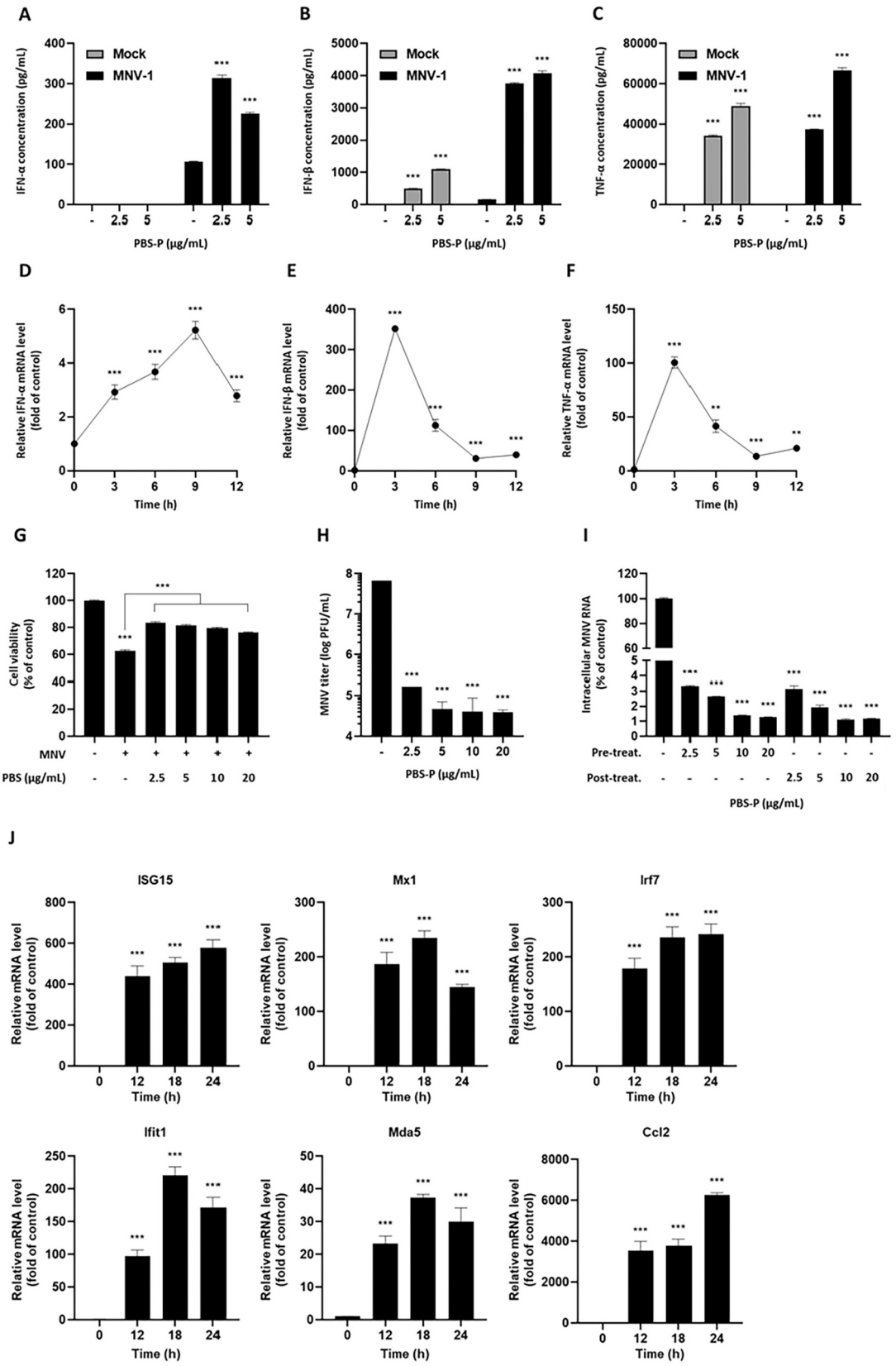

Fig. 5. PBS-P prevents MNV infection through increased expression of interferon-stimulated genes (ISGs).
(A-C) Mock-infected or MNV (MOI of 0.05) infected RAW 264.7 cells were treated with the PBS-P for 24 h. The protein levels of (A) IFN-α, (B) IFN-β and (C) TNF-α were measured using ELISA. (D—F) The cells were treated with PBS-P (20 μg/mL), and the mRNA levels of (D) IFN-α, (E) IFN-β and (F) TNF-α were quantified by RT-qPCR. (G-I) The cells were infected with MNV (MOI of 0.05) and treated with PBS-P for 24 h postinfection. (G) Cell viability was measured using SRB assay. (H) MNV titers were determined using a plaque forming assay. (I) Intracellular MNV RNA titers were quantified by RT-qPCR. (J) The mRNA level changes of ISGs after treatment PBS-P (20 μg/mL) were quantified by RT-qPCR. Data are shown as mean ± SD. $^{**}P < 0.01$ and $^{***}P < 0.001$.

[→4,6)-α-D-Glc*p*-(1 → 4)-α-D-Glc*p*-(1→], indicating a linear backbone structure of PBS-P (Zhang et al., 2018).

Moreover, the correlation peaks from H1 of residues E (δ_H 5.48 ppm), and G (δ_H 5.25 ppm), linked to the C6 of residue A (δ_C 62.91 ppm), indicated the substitution of residue A at the O-6 position by Rha*p*, and terminal Glc*p* residues, respectively. Furthermore, HMBC correlation peaks from H1 of H residue (δ_H 4.96 ppm) and C4 of residues A/B (δ_C 73.0 ppm) indicated the presence of →4)-α-D-Glc*p*A-(1 → 4)-α-D-Glc*p*-(1 → (Zhao et al., 2023).

The correlations observed between H1 of residues A/B (δ_H 5.68 and 5.66 ppm) with C3 of residue C (δ_C 77.3 ppm) and C4 of residue D (δ_C 76.85 ppm) suggested the presence of non-branched [→4)-α-D-Glc*p*-(1 → 3)-α-D-Gal*p*-(1→] and [→4)-α-D-Glc*p*-(1 → 4)-α-D-Man*p*-(1→] fragments, respectively, attached along the backbone of PBS-P. The H1 of residue F (δ_H 5.16 ppm) also correlated with the C2 of residue E (δ_C 70.2 ppm), implying that residue E was terminated at the O-2 position by residue F (T-α-L-Ara*p*-(1→).

Based on the results, PBS-P was identified as an α-glycosidic configurated acidic heteroglycan, with structural units composed predominantly of repeating units of →4)-α-D-Glc*p*-(1 → 4,6)-α-D-Glc*p*-(1→, →4)-α-D-Glc*p*A-(1→, →3)-α-L-Rha*p*-(1→, →3)-α-D-Gal*p*-(1 → and →4)-α-D-Man*p*-(1→, branched at the 6-position of 1,4,6-linked-Glc*p* with →1)-α-L-Rha*p*-(2 → 1)-α-L-Ara*p*-(1→, and terminal α-D-Glc*p*-(1 → residues. Previous studies have reported acidic heteroglycans with primarily α-glycosidic linkages isolated from *Polygonum multiflorum* (Zhang et al., 2018), β-glycosidic linkages from *Ganoderma lucidum* (Chen et al., 2022), and a combination of both α- and β-glycosidic linkages from *Tricholoma lobayense* (Mehmood et al., 2019). However, reports on the structural characterization of purified polysaccharides from PBSL are currently unavailable. Although the monosaccharide constituents of PBS-P in this study is similar to the purified polysaccharide from melon fly (*Bactrocera cucurbitae*) pupae (Ohta et al., 2014), variations exist in their structural configurations. To the best of our knowledge, this is the first study on the purification and detailed structural characterization of a polysaccharide from edible insects. In agreement with the PBS-P structure, acidic heteroglycans isolated from other sources such as mushrooms and herbal plants have demonstrated potent biological activities, including immunomodulatory effects (Chen et al., 2022; He et al., 2016; Ohta et al., 2014; Zeb et al., 2021; Zhao et al., 2023).

3.3. Comparative evaluation of antiviral activity of PBS-P and PBSE against MNV infection

To confirm whether PBS-P exhibits superior antiviral effects against MNV compared to PBSE, we first compared the production capacities of IFN-β which plays a crucial role in triggering antiviral innate immune responses, and TNF-α which promotes the production of IFN-β and enhances innate immune responses, at multiple concentrations for PBS-P (4 to 20 μg/mL) and PBSE (4 to 100 μg/mL). At the concentrations tested, PBS-P did not affect the cell viability of RAW 264.7 cells, indicating its non-cytotoxicity (Fig. 4A). At the concentration of 20 μg/mL, PBS-P treatment induced approximately 80-fold higher IFN-β levels and 15-fold higher TNF-α levels compared to PBSE treatment (Fig. 4B, C).

Similarly, under MNV infection conditions, PBS-P treatment induced IFN-β protein levels and TNF-α protein levels up to 22-fold and 66-fold higher, respectively, compared to PBSE treatment (Fig. 4D, E). Furthermore, we confirmed that PBS-P treatment resulted in significantly lower levels of viral titers compared to PBSE treatment in the plaque-forming assay (Fig. 4F).

In contrast to previous reports (J. Lee et al., 2017; J. H. Lee et al., 2023), our findings suggest that polysaccharides are a major immunomodulatory component in PBSE, and the purified fraction eluted with 0.5 M NaCl solution (PBS-P) is likely the active component responsible for the antiviral immune effects exerted by PBSE. To further investigate the underlying mechanism of its antiviral properties, PBS-P was subjected to *in vitro* and *in vivo* experiments.

3.4. PBS-P exerts antiviral activity through activating interferon-stimulated genes

To assess the antiviral activity of PBS-P against MNV, we examined the effects of PBS-P on type 1 interferons, IFN-α and IFN-β, and TNF-α production in macrophages under MNV-infection conditions. PBS-P induced IFN-β and TNF-α protein levels in both mock-infection and MNV-infection conditions and upregulated IFN-α protein levels under MNV-infection conditions (Fig. 5A-C). In addition, PBS-P treatment increased the mRNA levels of IFN-α, IFN-β, and TNF-α in macrophages (Fig. 5D-F).

MNV infection is known to cause apoptosis through cytopathic effects (Deerain et al., 2024). Therefore, to examine the protective effect of PBSE against host cell death mediated by MNV, we measured cell viability after MNV infection in macrophages. PBS-P treatment restored the MNV-mediated reduction in cell viability from 62.7 % to 83.4 % (Fig. 5G) and significantly reduced the viral load by up to 1600-fold in the plaque-forming assay (Fig. 5H). Having confirmed the antiviral activity of PBS-P against MNV, we subsequently decided to investigate at which stage PBS-P acts during MNV infection. Using RT-qPCR, we quantified the intracellular MNV RNA level. After MNV infection, posttreatment of PBS-P reduced the viral load by 98.2 %, and the pretreatment of PBS-P before MNV infection did not lead to a further reduction in viral load compared to posttreatment (Fig. 3I). These results suggest that PBS-P enhances the host cell defense mechanism against MNV infection rather than inhibiting the entry stage of viral infection. The results suggest that PBS-P enhances the host cell's antiviral defense mechanisms rather than inhibiting the viral entry stage (Fig. 5I). These results suggest that PBS-P enhances the host cell defense mechanism against MNV infection rather than inhibiting the entry stage of viral infection. As PBS-P markedly reduced viral loads and upregulated type 1 interferon levels, we analyzed the expression of interferon-stimulated genes (ISGs). We observed that PBS-P treatment profoundly increased mRNA expression levels of ISGs (Isg15, Mx1, Irf7, Ifit1, Mda5, Ccl2), which are induced by type 1 IFN and are known to be the ultimate effectors of host cell defense mechanism against viral infection (Yang & Li, 2020) (Fig. 5J). These results indicate that PBS-P enhances the host cell's antiviral mechanisms by upregulating the transcription of various ISGs through increased production of type 1 IFN and TNF-α in virus-infected cells.

The observed antiviral effects of PBS-P are consistent with the immunomodulatory properties reported for other plant-derived polysaccharides. These polysaccharides can exhibit antiviral activity through multiple mechanisms, including enhancing the host's immune response and directly interfering with viral entry and replication (Andrew & Jayaraman, 2021; Mohanta et al., 2023). For instance, the acidic *Houttuynia cordata* polysaccharide was shown to reduce the residual infectivity of murine norovirus-1 (MNV-1) by altering the morphology of the viral particles, thereby inhibiting virus penetration and internalization into the host cells (Cheng et al., 2019). Additionally, the anionic nature of certain polysaccharides has been reported to interfere with the attachment of viruses, such as human papillomavirus (HPV) and cytomegalovirus (CMV), to their target cells (Martinez et al., 2005). The polysaccharides can interact with the positively charged amino acid domains of cell surface glycoproteins, providing a shielding effect that prevents the binding of the virus to the host cell (Gao et al., 2018).

3.5. Molecular mechanism of PBS-P for its antiviral activity

We further investigated the underlying molecular mechanism responsible for the antiviral activity of PBS-P. We examined the effect of PBS-P on NF-κB and IRF3 which can act as transcription factors for the expression of IFN-α, IFN-β, and TNF-α (Lukhele et al., 2019). In addition, it has been reported that the NF-κB signaling pathway can assist in the activation of IRFs and the expression of type 1 IFN genes (Y.-S. Lee et al., 2021). PBS-P treatment induced phospho-IκBα and phospho-NF-κB,

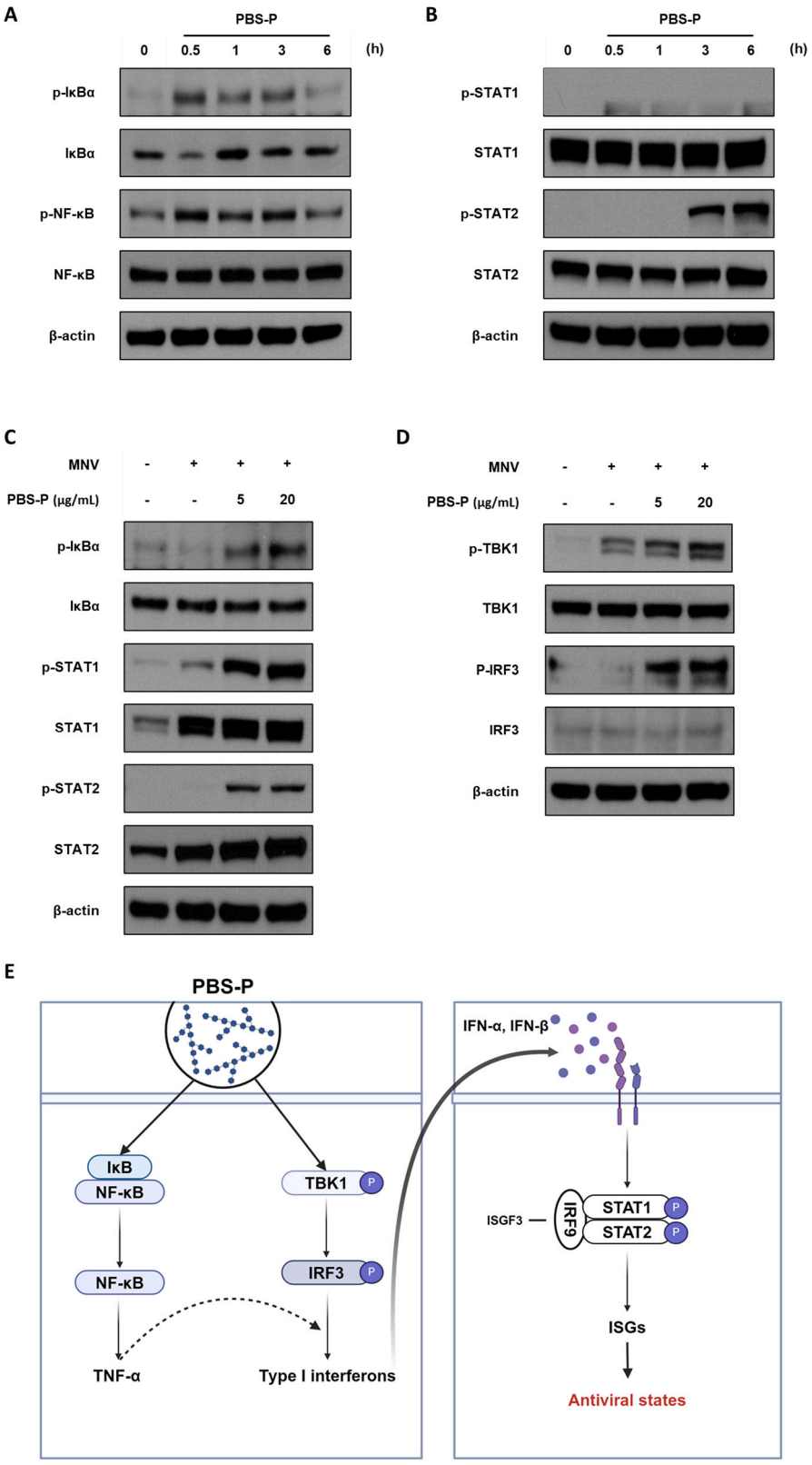

Fig. 6. PBS-P activates NF-κB, STAT1/2 and TBK-IRF3 pathways.
(A and B) The RAW 264.7 cells were treated with PBS-P (20 μg/mL) for indicated time. Protein expression levels of phosphorylated and total (A) STAT1 and STAT2, (B) IκBα and NF-κB were determined by western blotting. (C and D) MNV-infected (MOI of 0.0.05) RAW 264.7 cells were treated with indicated concentration of PBS-P for 6 h. Protein levels of phosphorylated and total (C) IκBα, STAT1 and STAT2, (D) TBK1 and IRF3 were determined by western blotting. (E) Schematic diagram summarizing the molecular mechanism of PBS-P.

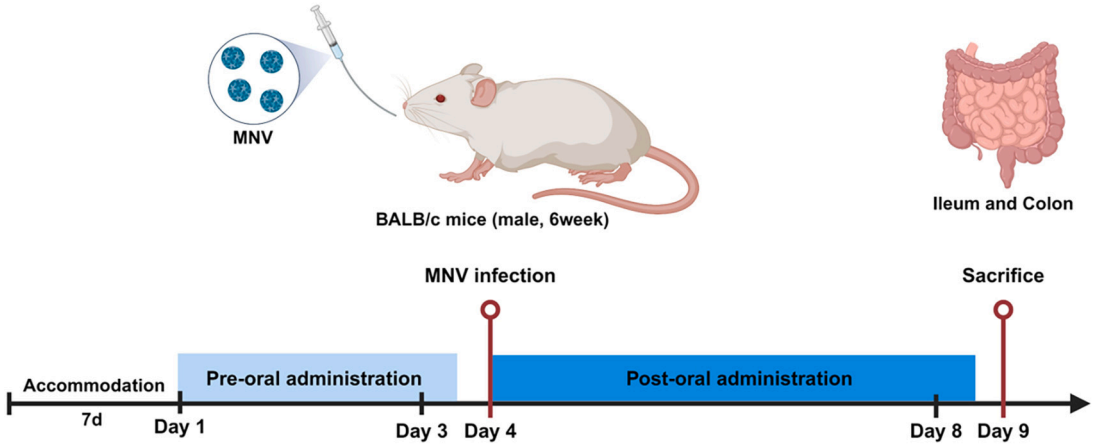

Fig. 7. Schema of the experimental design of *in vivo* MNV replication reduction studies.
BALB/c mice (6 weeks old, male) were infected with MNV by peroral inoculation, and PBS-P (75 mg/kg of body weight) was administered once a day for 8 d. On day 9, the mice were sacrificed, and their ileum and colon tissues were collected (created with BioRender.com).

Table 5
Effect PBS-P treatment on MNV genome level *in vivo*.

Groups	MNV genome copies (per μg DNA)	
	Ileum	Colon
Control	1285.6 ± 227.5	6118.758 ± 631.0
MNV	64,862.4 ± 4871.8	42,624.54 ± 6025.2
MNV + PBS-P	22,190.3 ± 7554.0	13,912.12 ± 1964.5

MNV genome copies in ileum tissue extract and colon tissue extract were quantified by RT-qPCR. Data were analyzed by the Mann-Whitney test. Data are shown as mean ± SEM ($n = 5$), and $P < 0.01$.

peaking at 0.5 h **(**Fig. 6A and **Fig. S7A)**. When type 1 IFN binds to IFN receptors, it activates the Janus kinase (JAK)-STAT pathway. Phosphorylated STAT1 and STAT2 form the ISG factor 3 complex (ISGF3) with IRF9 and directly induce the transcription of antiviral interferon-stimulated genes (McNab et al., 2015). PBS-P treatment elevated the levels of phosphorylated STAT1 and STAT2, peaking at 6 h (Fig. 6B and **Fig. S7B**). To identify the effect of PBS-P under the viral infection conditions, we analyzed the same signaling pathway during MNV infection. After infection, PBS-P treatment increased the phosphorylation levels of IκBα, STAT1, and STAT2 compared to MNV infection alone (Fig. 6C and **Fig. S7C**). In addition, the phosphorylation levels of TBK1 and IRF3 which were direct transcription factors of IFN-β, exhibited a dose-dependent increase upon PBS-P treatment (Fig. 6D and **Fig. S7D**). Collectively, these results demonstrate that PBS-P activates NF-κB and IRF3 pathways to express IFN-α and IFN-β. Upregulated IFNs in turn promote phosphorylation of STAT1/2 leading to the expression of ISGs, promoting antiviral immune reactions (Fig. 6E).

These results suggest that the enhanced antiviral effect of PBS-P in host cells against MNV occurs through the activation of type 1 interferon transcription factors and the transcription of interferon-stimulated genes (ISGs) mediated by the activation of the JAK-STAT signaling pathway. This is consistent with the reported antiviral mechanisms of polysaccharides from other natural sources, such as *Morehella esculenta* and *Enteromorpha prolifera*, which can modulate the immune response through the activation of signaling pathways involving Akt/NF-κB, and the upregulation of cytokines like IFN (J.-K. Kim et al., 2011; Wen et al., 2019).

3.6. Antiviral activity of PBS-P against MNV in vivo

Noroviruses are reported to infect the small intestine and large intestine, particularly targeting the ileum and colon areas (Graziano et al., 2021; Wilen et al., 2018). Therefore, we investigated whether orally administered PBS-P could suppress MNV infection in the ileum and colon. Mice were infected with MNV by peroral inoculation, and PBS-P (75 mg/kg of body weight) was administered for 8 days starting from 3 days before infection (Fig. 7 **A**). To assess the inhibitory effect on MNV infection, viral RNA levels were examined by RT-qPCR in the ileum and colon tissues. Mice administered with PBS-P displayed 65.8 % lower MNV genome levels in the ileum tissue compared to the vehicle-treated mice. Similarly, 67.4 % lower MNV genome levels were observed in the colon tissues of PBS-P treated mice (Table 5**)**. These results suggest that oral administration of PBS-P can inhibit MNV infection in the intestinal tissues.

4. Conclusion

In this study, PBS-P, an α-configurated acidic branched heteroglycan from *Protaetia brevitarsis seulensis* larvae was successfully isolated and characterized, demonstrating its potent antiviral activity against murine norovirus (MNV). This study advances beyond the previous reports on bioactive components from PBSL and other insects, which had not sufficiently suggested the chemical structure of bioactive components. It is the first discovery to elucidate the substantial structure of the bioactive component through intensive analysis of spectroscopic data from a polysaccharide of an insect. PBS-P enhanced host cell defense mechanisms by activating NF-κB, STAT1/2, and TBK1-IRF3 signaling pathways, and its oral administration significantly reduced MNV genome copy numbers in the ileum and colon of infected mice. These findings provide key insights into antiviral polysaccharides from insect sources, supporting the development of functional foods with therapeutic properties from edible insects. However, the exact biosynthetic pathways and the role of gut microbiota in polysaccharide production in PBSL remain unclear. Future research could focus on elucidating these mechanisms and exploring how different dietary sources influence PBSL polysaccharides' composition and bioactivity. Additionally, studies investigating PBS-P's efficacy against other viral systems and clinical trials are necessary to explore the potential of PBS-P as an effective natural antiviral agent.

CRediT authorship contribution statement

Ibukunoluwa Fola Olawuyi: Writing – original draft, Methodology, Data curation, Conceptualization. **Eun Heo:** Writing – original draft, Methodology, Data curation. **Minju Jeong:** Methodology. **Jong-Jin Park:** Methodology, Investigation. **Jongbeom Chae:** Methodology, Data curation. **Subin Gwon:** Methodology, Investigation. **Seong Do Lee:** Methodology, Investigation. **Hunseong Kim:** Methodology,

Investigation. **Oyindamola Vivian Ojulari:** Writing – review & editing. **Young-Bo Song:** Methodology. **Byung-Hoo Lee:** Methodology. **Bon Bin Gu:** Methodology, Data curation. **Soo Rin Kim:** Methodology, Data curation. **Joon Ha Lee:** Resources, Investigation. **Wonyoung Lee:** Resources, Investigation. **Jae Sam Hwang:** Methodology. **Ju-Ock Nam:** Resources, Investigation. **Dongyup Hahn:** Writing – review & editing, Supervision, Resources, Project administration, Investigation, Funding acquisition. **Sanguine Byun:** Writing – review & editing, Supervision, Resources, Project administration, Investigation, Funding acquisition, Conceptualization.

Declaration of competing interest

The authors declare that they have no known competing financial interests or personal relationships that could have appeared to influence the work reported in this paper.

Data availability

The authors do not have permission to share data.

Acknowledgements

This work was supported by Korea Basic Science Institute (National Research Facilities and Equipment Center) funded by the Ministry of Education (2021R1A6C101A416), and Biological Materials-Specialized Graduate Program through the Korea Environmental Industry & Technology Institute (KEITI) funded by the Ministry of Environment (MOE).

Funding resources

This research was supported by Rural Development Administration (PJ01594003), and National Research Foundation (NRF), funded by the Korean government (MSIT) (2023R1A2C1006827).

Appendix A. Supplementary data

Supplementary data to this article can be found online at https://doi.org/10.1016/j.carbpol.2024.122587.

References

Akbari, A., Bigham, A., Rahimkhoei, V., Sharifi, S., & Jabbari, E. (2022). *Antiviral polymers: a review. Polymers, 14*, 1634.

Ali, M. F. Z., Yasin, I. A., Ohta, T., Hashizume, A., Ido, A., Takahashi, T., … Miura, T. (2018). The silkrose of Bombyx mori effectively prevents vibriosis in penaeid prawns via the activation of innate immunity. *Scientific Reports, 8*, 8836.

Andrew, M., & Jayaraman, G. (2021). Marine sulfated polysaccharides as potential antiviral drug candidates to treat Corona virus disease (COVID-19). *Carbohydrate Research, 505*, Article 108326.

Atmar, R. L., Ramani, S., & Estes, M. K. (2018). Human noroviruses: Recent advances in a 50-year history. *Current Opinion in Infectious Diseases, 31*, 422–432.

Chen, S., Guan, X., Yong, T., Gao, X., Xiao, C., Xie, Y., Chen, D., Hu, H., & Wu, Q. (2022). Structural characterization and hepatoprotective activity of an acidic polysaccharide from Ganoderma lucidum. *Food Chemistry: X, 13*, Article 100204.

Cheng, D., Sun, L., Zou, S., Chen, J., Mao, H., Zhang, Y., … Zhang, R. (2019). Antiviral effects of *Houttuynia cordata* polysaccharide extract on murine Norovirus-1 (MNV-1)—A human norovirus surrogate. *Molecules, 24*, 1835.

Cho, H. G., Lee, S. G., Lee, M. Y., Hur, E. S., Lee, J. S., Park, P. H., … Paik, S. Y. (2016). An outbreak of norovirus infection associated with fermented oyster consumption in South Korea, 2013. *Epidemiology and Infection, 144*, 2759–2764.

Choi, R.-Y., Kim, I.-W., Ji, M., Paik, M.-J., Ban, E.-J., Lee, J. H., … Seo, M. (2023). *Protaetia brevitarsis seulensis* larvae ethanol extract inhibits RANKL-stimulated osteoclastogenesis and ameliorates bone loss in ovariectomized mice. *Biomedicine & Pharmacotherapy, 165*, Article 115112.

Claus-Desbonnet, H., Nikly, E., Nalbantova, V., Karcheva-Bahchevanska, D., Ivanova, S., Pierre, G., & Lukova, P. (2022). Polysaccharides and their derivatives as potential antiviral molecules. *Viruses, 14*(2), 426.

Dai, J., Wu, Y., Chen, S.-w., Zhu, S., Yin, H.-p., Wang, M., & Tang, J. (2010). Sugar compositional determination of polysaccharides from *Dunaliella salina* by modified RP-HPLC method of precolumn derivatization with 1-phenyl-3-methyl-5-pyrazolone. Carbohydrate Polymers, 82, 629–635.

Deerain, J. M., Aktepe, T. E., Trenerry, A. M., Ebert, G., Hyde, J. L., Charry, K., … Mackenzie, J. M. (2024). Murine norovirus infection of macrophages induces intrinsic apoptosis as the major form of programmed cell death. *Virology, 589*, Article 109921.

Filisetti-Cozzi, T. M., & Carpita, N. C. (1991). Measurement of uronic acids without interference from neutral sugars. *Analytical Biochemistry, 197*, 157–162.

Gao, Y., Liu, W., Wang, W., Zhang, X., & Zhao, X. (2018). The inhibitory effects and mechanisms of 3, 6-O-sulfated chitosan against human papillomavirus infection. *Carbohydrate Polymers, 198*, 329–338.

Giraud, M.-F., & Naismith, J. H. (2000). The rhamnose pathway. *Current Opinion in Structural Biology, 10*, 687–696.

Gonzalez-Hernandez, M. B., Cunha, J. B., & Wobus, C. E. (2012). Plaque assay for murine norovirus. *Jove-Journal of Visualized Experiments, 66*, Article e4297.

Graziano, V. R., Alfajaro, M. M., Schmitz, C. O., Filler, R. B., Strine, M. S., Wei, J., … Orchard, R. C. (2021). CD300lf conditional knockout mouse reveals strain-specific cellular tropism of murine norovirus. *Journal of Virology, 95*, 10–1128.

He, P., Zhang, A., Zhang, F., Linhardt, R. J., & Sun, P. (2016). Structure and bioactivity of a polysaccharide containing uronic acid from Polyporus umbellatus sclerotia. *Carbohydrate Polymers, 152*, 222–230.

Huang, Y., Ye, Y., Xu, D., Ji, J., Sun, J., Xu, M., Xia, B., Shen, H., Xia, R., Shi, W., & Sun, X. (2023). Structural characterization and anti-inflammatory activity of a novel neutral polysaccharide isolated from *Smilax glabra* Roxb. *International Journal of Biological Macromolecules, 234*, Article 123559.

Jo, S., Samarpita, S., Lee, J. S., Lee, Y. J., Son, J. E., Jeong, M., Kim, J. H., Hong, S., Yoo, S.-A., Kim, W.-U, Rasool, M., & Byun, S. (2022). 8-Shogaol inhibits rheumatoid arthritis through targeting TAK1. Pharmacological Research, 178, 106176.

Kang, M., Kang, C., Lee, H., Kim, E., Kim, J., Kwon, O., Lee, H., Kang, H., Kim, C., & Jang, H. (2012). Effects of fermented *aloe vera* mixed diet on larval growth of *Protaetia brevitarsis seulensis* (Kolbe)(coleopteran: Cetoniidae) and protective effects of its extract against CCl4-induced hepatotoxicity in Sprague–Dawley rats. Entomological Research, 42, 111–121.

Karst, S. M., Wobus, C. E., Goodfellow, I. G., Green, K. Y., & Virgin, H. W. (2014). Advances in norovirus biology. *Cell Host & Microbe, 15*, 668–680.

Kim, D., Jeong, M., Kim, J. H., Son, J. E., Lee, J. J. Y., Park, S. J., Lee, J.,Kim, M., Oh, J.-W., Park, M. S., Byun, S. (2022a). Lactobacillus salivarius HHuMin-U activates innate immune defense against norovirus infection through TBK1-IRF3 and NF-KB signaling pathways. Research, 2022, 0007.

Kim, D. H., Kim, J. H., Jo, J. Y., & Byun, S. (2022). Functional foods with antiviral activity. *Food Science and Biotechnology, 31*, 527–538.

Kim, J.-K., Cho, M. L., Karnjanapratum, S., Shin, I.-S., & You, S. G. (2011). In vitro and in vivo immunomodulatory activity of sulfated polysaccharides from *Enteromorpha prolifera*. *International Journal of Biological Macromolecules, 49*, 1051–1058.

Kwon, E.-Y., Yoo, J., Yoon, Y.-I., Hwang, J.-S., Goo, T.-W., Kim, M.-A., Choi, Y.-C., & Yun, E.-Y. (2013). Pre-treatment of the white-spotted flower chafer (Protaetia brevitarsis) as an ingredient for novel foods. *Journal of the Korean Society of Food Science and Nutrition, 42*, 397–402.

Lee, J., Lee, W., Kim, M. A., Hwang, J. S., Na, M., & Bae, J. S. (2017). Inhibition of platelet aggregation and thrombosis by indole alkaloids isolated from the edible insect *Protaetia brevitarsis seulensis* (Kolbe). *Journal of Cellular and Molecular Medicine, 21*, 1217–1227.

Lee, J. H., Kim, T.-K., Kim, Y. J., Kang, M.-C., Song, K.-M., Kim, B.-K., & Choi, Y.-S. (2023). Structural, physicochemical, and immune-enhancing properties of edible insect protein isolates from *Protaetia brevitarsis* larvae. *Food Chemistry: X, 18*, Article 100722.

Lee, Y.-S., Bao, X., Lee, H.-H., Jang, J. J., Saruuldalai, E., Park, G., … Lee, Y. S. (2021). Nc886, a novel suppressor of the type I interferon response upon pathogen intrusion. *International Journal of Molecular Sciences, 22*, 2003.

Lin, X.-t., Xiao, B.-x., Liu, J.-p., Cao, M.-y., Yang, Z.-p., Zhao, L.-y., & Chen, G.-t. (2023). An acidic heteropolysaccharide rich in galactose and arabinose derived from ginger: Structure and dynamics. *Food Bioscience, 56*, Article 103127.

Liu, D., Tang, W., Yin, J.-Y., Nie, S.-P., & Xie, M.-Y. (2021). Monosaccharide composition analysis of polysaccharides from natural sources: Hydrolysis condition and detection method development. *Food Hydrocolloids, 116*, Article 106641.

Liu, Y., Ye, Y., Hu, X., & Wang, J. (2021). Structural characterization and anti-inflammatory activity of a polysaccharide from the lignified okra. *Carbohydrate Polymers, 265*, Article 118081.

Lukhele, S., Boukhaled, G. M., & Brooks, D. G. (2019). Type I interferon signaling, regulation and gene stimulation in chronic virus infection. *Seminars in immunology* (Vol. 43, p. 101277): Elsevier.

Maity, P., Nandi, A. K., Manna, D. K., Pattanayak, M., Sen, I. K., Bhanja, S. K., … Islam, S. S. (2017). Structural characterization and antioxidant activity of a glucan from *Meripilus giganteus*. *Carbohydrate Polymers, 157*, 1237–1245.

Manna, D. K., Maity, P., Nandi, A. K., Pattanayak, M., Panda, B. C., Mandal, A. K., … Islam, S. S. (2017). Structural elucidation and immunostimulating property of a novel polysaccharide extracted from an edible mushroom *Lentinus fusipes*. *Carbohydrate Polymers, 157*, 1657–1665.

Martinez, M. J. A., Del Olmo, L. M. B., & Benito, P. B. (2005). Antiviral activities of polysaccharides from natural sources. *Studies in Natural Products Chemistry, 30*, 393–418.

Mboko, W. P., Chhabra, P., Valcarce, M. D., Costantini, V., & Vinjé, J. (2022). Advances in understanding of the innate immune response to human norovirus infection using organoid models. *Journal of General Virology, 103*, Article 001720.

McNab, F., Mayer-Barber, K., Sher, A., Wack, A., & O'Garra, A. (2015). Type I interferons in infectious disease. *Nature Reviews Immunology, 15*, 87–103.

Mehmood, S., Zhou, L.-Y., Wang, X.-F., Cheng, X.-D., Meng, F.-J., Wang, Y., … Chen, Y. (2019). Structural elucidation and antioxidant activity of a novel heteroglycan from *Tricholoma Lobayense*. *Journal of Carbohydrate Chemistry, 38*, 192–211.

Mohanta, B., Nayak, A. K., & Dhara, A. K. (2023). Plant polysaccharides as antiviral agents. In *Viral infections and antiviral therapies* (pp. 567–579). Elsevier.

Ohta, T., Ido, A., Kusano, K., Miura, C., & Miura, T. (2014). A novel polysaccharide in insects activates the innate immune system in mouse macrophage RAW264 cells. *PLoS One, 9*, Article e114823.

Ohta, T., Kusano, K., Ido, A., Miura, C., & Miura, T. (2016). Silkrose: A novel acidic polysaccharide from the silkmoth that can stimulate the innate immune response. *Carbohydrate Polymers, 136*, 995–1001.

Olawuyi, I. F., & Lee, W. Y. (2021). Structural characterization, functional properties and antioxidant activities of polysaccharide extract obtained from okra leaves (*Abelmoschus esculentus*). *Food Chemistry, 354*, Article 129437.

Pettolino, F. A., Walsh, C., Fincher, G. B., & Bacic, A. (2012). Determining the polysaccharide composition of plant cell walls. *Nature Protocols, 7*, 1590–1607.

Qi, W., Zhou, X., Wang, J., Zhang, K., Zhou, Y., Chen, S., Nie, S., & Xie, M. (2020). *Cordyceps sinensis* polysaccharide inhibits colon cancer cells growth by inducing apoptosis and autophagy flux blockage via mTOR signaling. *Carbohydrate Polymers, 237*, Article 116113.

Shi, Y., He, X., Bai, B., Wang, H., Liu, C., Xue, L., Wu, J., Wu, Y., & Zheng, C. (2023). Structural characterization and antinociceptive activity of polysaccharides from *Anoectochilus elatus*. *International Journal of Biological Macromolecules, 233*, Article 123542.

Sims, I. M., Carnachan, S. M., Bell, T. J., & Hinkley, S. F. (2018). Methylation analysis of polysaccharides: Technical advice. *Carbohydrate Polymers, 188*, 1–7.

Stepan, H., & Staudacher, E. (2011). Optimization of monosaccharide determination using anthranilic acid and 1-phenyl-3-methyl-5-pyrazolone for gastropod analysis. *Analytical Biochemistry, 418*, 24–29.

Tabarsa, M., You, S., Yelithao, K., Palanisamy, S., Prabhu, N. M., & Nan, M. (2020). Isolation, structural elucidation and immuno-stimulatory properties of polysaccharides from *Cuminum cyminum*. *Carbohydrate Polymers, 230*, Article 115636.

Wen, Y., Peng, D., Li, C., Hu, X., Bi, S., Song, L., Peng, B., Zhu, J., Chen, Y., & Yu, R. (2019). A new polysaccharide isolated from Morchella importuna fruiting bodies and its immunoregulatory mechanism. *International Journal of Biological Macromolecules, 137*, 8–19.

Wilen, C. B., Lee, S., Hsieh, L. L., Orchard, R. C., Desai, C., Hykes, B. L., Jr., … A., Cadwell, K., Allen, P. M., Handley, S. A., Van Lookeren Campagne, M., Baldridge, M. T., & Virgin, H. W.. (2018). Tropism for tuft cells determines immune promotion of norovirus pathogenesis. *Science, 360*(6385), 204–208.

Wobus, C. E., Karst, S. M., Thackray, L. B., Chang, K. O., Sosnovtsev, S. V., Belliot, G., … Virgin, H. W. (2004). Replication of *norovirus* in cell culture reveals a tropism for dendritic cells and macrophages. *PLoS Biology, 2*, 2076–2084.

Wu, Y., Zhou, H., Wei, K., Zhang, T., Che, Y., Nguyễn, A. D., … Wu, Y. (2022). Structure of a new glycyrrhiza polysaccharide and its immunomodulatory activity. *Frontiers in Immunology, 13*, 1007186.

Yang, E., & Li, M. (2020). All about the RNA: Interferon-stimulated genes that interfere with viral RNA processes. *Frontiers in Immunology, 11*, Article 605024.

Yin, Z.-H., Liu, X.-P., Wang, J.-M., Xi, X.-F., Zhang, Y., Zhao, R.-L., & Kang, W.-Y. (2022). Structural characterization and anticoagulant activity of a 3-O-methylated Heteroglycan from fruiting bodies of *Pleurotus placentodes*. *Frontiers in Chemistry, 10*, Article 825127.

Zarubova, J., Zhang, X., Hoffman, T., Hasani-Sadrabadi, M. M., & Li, S. (2021). Biomaterial-based immunoengineering to fight COVID-19 and infectious diseases. *Matter, 4*, 1528–1554.

Zeb, M., Tackaberry, L. E., Massicotte, H. B., Egger, K. N., Reimer, K., Lu, G., … Lee, C. H. (2021). Structural elucidation and immuno-stimulatory activity of a novel polysaccharide containing glucuronic acid from the fungus *Echinodontium tinctorium*. *Carbohydrate Polymers, 258*, Article 117700.

Zhang, Q., Xu, Y., Lv, J., Cheng, M., Wu, Y., Cao, K., Zhang, X., Mou, X., & Fan, Q. (2018). Structure characterization of two functional polysaccharides from *Polygonum multiflorum* and its immunomodulatory. *International Journal of Biological Macromolecules, 113*, 195–204.

Zhao, S., Xue, H., Tao, Y., Chen, K., Li, X., & Wang, M. (2023). An acidic Heteropolysaccharide isolated from *Pueraria lobata* and its bioactivities. *International Journal of Molecular Sciences, 24*, 6247.

Update 1 of 2

Carbohydrate Polymers

Volume 351, Issue , 1 March 2025, Page

DOI: https://doi.org/10.1016/j.carbpol.2024.123127

Carbohydrate Polymers 351 (2025) 123127

Contents lists available at ScienceDirect

Carbohydrate Polymers

journal homepage: www.elsevier.com/locate/carbpol

Corrigendum

Corrigendum to "Acidic polysaccharide from the edible insect *Protaetia brevitarsis seulensis* activates antiviral immunity to suppress norovirus infection" [Carbohydrate Polymers, Volume 347 (2025), Article Number 122587]

Ibukunoluwa Fola Olawuyi [a,e,1], Eun Heo [b,1], Minju Jeong [c], Jae Hwan Kim [b], Jong-Jin Park [d], Jongbeom Chae [e], Subin Gwon [f], Seong Do Lee [e], Hunseong Kim [e], Oyindamola Vivian Ojulari [e], Young-Bo Song [g], Byung-Hoo Lee [g], Bon Bin Gu [e], Soo Rin Kim [a,e], Joon Ha Lee [h], Wonyoung Lee [a,e], Jae Sam Hwang [i], Ju-Ock Nam [a,e], Dongyup Hahn [e,f,*], Sanguine Byun [b,j,**]

[a] *Research Institute of Tailored Food Technology, Kyungpook National University, Daegu 41566, Republic of Korea*
[b] *Department of Biotechnology, Yonsei University, Seoul 03722, Republic of Korea*
[c] *Department of Agricultural Biotechnology, Seoul National University, Seoul 08826, Republic of Korea*
[d] *Food Safety and Distribution Research Group, Korea Food Research Institute, Wanju-gun 55365, Republic of Korea*
[e] *School of Food Science and Biotechnology, College of Agriculture and Life Sciences, Kyungpook National University, Daegu 41566, Republic of Korea*
[f] *Department of Integrative Biotechnology, Kyungpook National University, Daegu 41566, Republic of Korea*
[g] *Department of Food Science & Biotechnology, Gachon University, Seongnam 13120, Republic of Korea*
[h] *Department of Agricultural Biology, National Institute of Agricultural Sciences, Rural Development Administration, Wanju 55362, Republic of Korea*
[i] *MyoTecSci Inc., Seoul 02792, Republic of Korea*
[j] *POSTECH Biotech Center, Pohang University of Science and Technology (POSTECH), Pohang 37673, Republic of Korea*

The authors regret that an incorrect blot for p-STAT1 was included in Fig. 6B of the originally published article. The correct image is provided below. This error does not affect the study's results or conclusions.

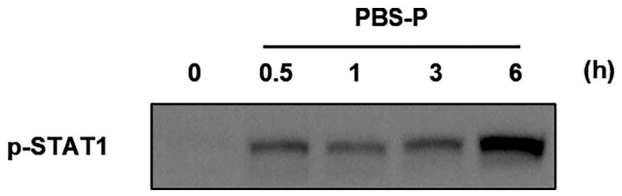

Also, Fig. 6 with the newly replaced p-STAT1 is provided below.

DOI of original article: https://doi.org/10.1016/j.carbpol.2024.122587.
* Correspondence to: D. Hahn, School of Food Science and Biotechnology, College of Agriculture and Life Sciences, Kyungpook National University, Daegu 41566, Republic of Korea.
** Correspondence to: S. Byun, Department of Biotechnology, Yonsei University, Seoul 03722, Republic of Korea.
E-mail addresses: dohahn@knu.ac.kr (D. Hahn), sanguine@yonsei.ac.kr (S. Byun).
[1] These authors contributed equally to this work.

https://doi.org/10.1016/j.carbpol.2024.123127

Available online 14 December 2024

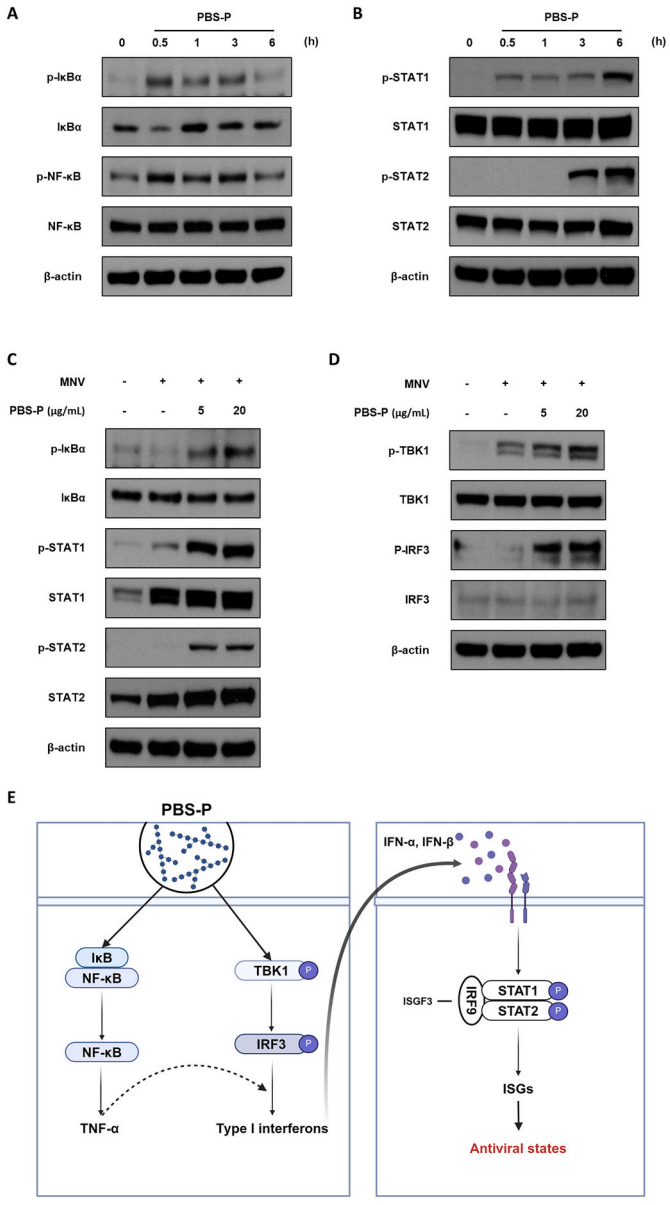

The authors would like to apologize for any inconvenience caused.

Update 2 of 2

Carbohydrate Polymers

Volume 352, Issue , 15 March 2025, Page

DOI: https://doi.org/10.1016/j.carbpol.2024.123188

Carbohydrate Polymers 352 (2025) 123188

Contents lists available at ScienceDirect

Carbohydrate Polymers

journal homepage: www.elsevier.com/locate/carbpol

Corrigendum

Corrigendum to "Acidic polysaccharide from the edible insect *Protaetia brevitarsis seulensis* activates antiviral immunity to suppress norovirus infection" [Carbohydrate Polymers 347 (2025) 122587]

Ibukunoluwa Fola Olawuyi [a,e,1], Eun Heo [b,1], Minju Jeong [c], Jae Hwan Kim [b], Jong-Jin Park [d], Jongbeom Chae [e], Subin Gwon [f], Seong Do Lee [e], Hunseong Kim [e], Oyindamola Vivian Ojulari [e], Young-Bo Song [g], Byung-Hoo Lee [g], Bon Bin Gu [e], Soo Rin Kim [a,e], Joon Ha Lee [h], Wonyoung Lee [a,e], Jae Sam Hwang [i], Ju-Ock Nam [a,e], Dongyup Hahn [e,f,*], Sanguine Byun [b,j,**]

[a] *Research Institute of Tailored Food Technology, Kyungpook National University, Daegu 41566, Republic of Korea*
[b] *Department of Biotechnology, Yonsei University, Seoul 03722, Republic of Korea*
[c] *Department of Agricultural Biotechnology, Seoul National University, Seoul 08826, Republic of Korea*
[d] *Food Safety and Distribution Research Group, Korea Food Research Institute, Wanju-gun 55365, Republic of Korea*
[e] *School of Food Science and Biotechnology, College of Agriculture and Life Sciences, Kyungpook National University, Daegu 41566, Republic of Korea*
[f] *Department of Integrative Biotechnology, Kyungpook National University, Daegu 41566, Republic of Korea*
[g] *Department of Food Science & Biotechnology, Gachon University, Seongnam 13120, Republic of Korea*
[h] *Department of Agricultural Biology, National Institute of Agricultural Sciences, Rural Development Administration, Wanju 55362, Republic of Korea*
[i] *MyoTecSci Inc., Seoul 02792, Republic of Korea*
[j] *POSTECH Biotech Center, Pohang University of Science and Technology (POSTECH), Pohang 37673, Republic of Korea*

The authors regret that an incorrect blot for p-STAT1 was included in Fig. 6B of the originally published article. The correct image is provided below. This error does not affect the study's results or conclusions.

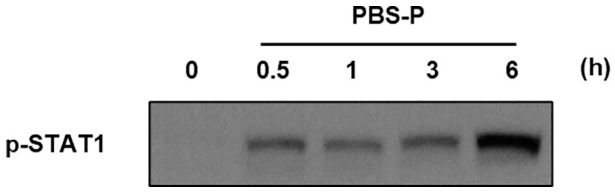

Also, Fig. 6 with the newly replaced p-STAT1 is provided below.

DOI of original article: https://doi.org/10.1016/j.carbpol.2024.122587.
* Correspondence to: D. Hahn, School of Food Science and Biotechnology, College of Agriculture and Life Sciences, Kyungpook National University, Daegu 41566, Republic of Korea.
** Correspondence to: S. Byun, Department of Biotechnology, Yonsei University, Seoul 03722, Republic of Korea.
E-mail addresses: dohahn@knu.ac.kr (D. Hahn), sanguine@yonsei.ac.kr (S. Byun).
[1] These authors contributed equally to this work.

https://doi.org/10.1016/j.carbpol.2024.123188

Available online 9 January 2025

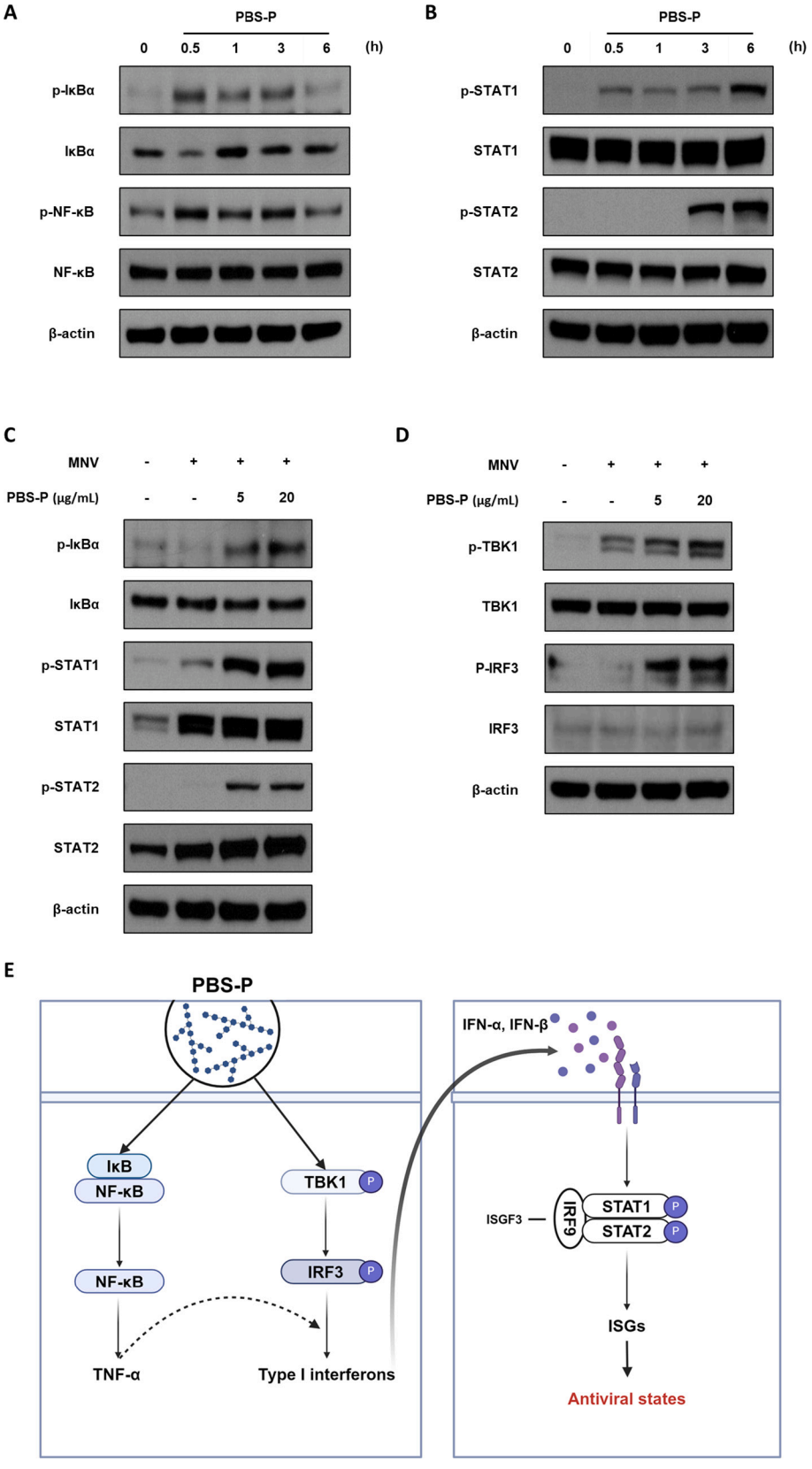

The authors would like to apologize for any inconvenience caused.